Geoinformatics & Geostatistics: An Overview

Research Article

A SCITECHNOL JOURNAL

Gaia, Revisited: Atmospheric CO_2 as a Symptom of a Vegetation Ozone Driven Climate Cycle

Isabel Van Waveren*

Department of NL Biodiversity and Society, Naturalis Biodiversity Centre, Leiden, The Netherlands

***Corresponding Author:** Isabel Van Waveren, Department of NL Biodiversity and Society, Naturalis Biodiversity Centre, Leiden, The Netherlands; E-mail: Isabel.VanWavren@gmail.com

Received date: 10 January, 2025, Manuscript No. GIGS-24-158405;

Editor Assigned date: 13 January, 2025, Pre QC No. GIGS-24-158405 (PQ);

Reviewed date: 27 January, 2025, QC No. GIGS-24-158405;

Revised date: 03 February, 2025, Manuscript No. GIGS-24-158405 (R);

Published date: 10 February, 2025, DOI: 10.4172/2327-4581.1000423.

Abstract

A synoptic analysis of the history of climate science introduces all potential climate drivers. This analysis is supported by demonstrating that the Global Carbon Equation (GCE) is not an equilibrium and the rapidly increasing atmospheric CO_2 concentrations recorded in the Keeling curve reflect yearly ocean CO_2 emission minus yearly ocean CO_2 uptake. Statistics are used to demonstrate that the increase in atmospheric CO_2 is correlated to industrial pollutant emission.

The significant determination coefficient between ocean behaviour and pollutants emission is interpreted as caused by pollutants accumulation in the Arctic night. With the return of light, in spring, the chemically reactive mixture of pollutants gas becomes self-lofting, thus influencing and being influenced by existing atmospheric pressure systems. The intensification results in storms that cause the thermocline to deepen and the ocean to degas.

The gases are argued to ascent to the stratosphere at the equator where they cause stratospheric ozone depletion, which in turn results in global warming. This new interpretation of the climate cycle is substantiated by a reconstruction of the Keeling curve consisting of the superposition of six functions that determine the uptake and emission of CO_2 by the Northern Pacific Ocean.

A regression analysis between the monthly Keeling curve and present reconstruction indicates that the new hypothesis is viable. Finally, it is shown that this situation reflects a response system between vegetation composition and stratospheric ozone that is driving the Pleistocene climate cycle through natural fire generated pollutants.

The present aberrantly high atmospheric CO_2 concentrations recorded at Mauna Loa are interpreted as resulting from the reiteration of the natural warming phase of the Pleistocene climate cycle just beyond the glacial maximum.

Keywords: Ozone; Ocean degassing; Particulates; Aerosols; Global warming; Mauna Loa; Keeling; Self-lofting; Fire; Charcoal.

Abbreviations: AMOC: Atlantic Mid Ocean Circulation; BCA: Black Carbon Aerosol; CCN: Cloud condensation nuclei; CFC: Chlorofluorocarbon; GCB: Global Carbon Budget; GCE: Global Carbon Equation; INP: Ice Nucleating Particles; IPCC: International Panel on Climate Change; NOAA: National Ocean and Atmospheric Administration; NPCE: Northern Pacific Carbon Equation; SCHWAB: Self-Lofting Chemically Reactive Arctic Winter Generated Air Bubble; SCHWOM: Self-lofting Chemically Reactive Warm Ocean Generated Air Mass; SOA: Secondary Organic Aerosols; VOC: Volatile Organic Carbon; WCRP: World Climate Research Program; E_{FOS}: Global Emission of CO_2 from the Burning of Fossil Energy Sources; E_{LUC}: Global Emission of CO_2 related to Land Use Change; E_{SLGHG}: Increase in Northern Pacific Ocean CO_2 Emission Caused by Short Lived Greenhouse Gas Accumulation; E_{SOD}: Global Ocean CO_2 Emission Caused by Stratospheric Ozone Depletion; E_{SOW}: Ocean CO_2 Emission in Atmospheric Caused by the Seasonal Ocean Warming Due to the Inclination of The Earth Axis; G_{ATM}: Global Atmospheric Growth In CO_2 Concentration; $G_{ATM\text{-}Here}$: Global Atmospheric Growth in CO_2 Concentration; $G_{ATM\text{-}WCRP}$: Global Atmospheric Growth in CO_2 concentration as Calculated by the World Climate Research Program; IE: $E_{FOS} + E_{LUC}$; ML_{YD}: Yearly Decrease in Atmospheric CO_2 Concentration as Measured by the NOAA at Mauna Loa; ML_{YI}: Yearly Increase in Atmospheric CO_2 Concentration as Measured by the NOAA at Mauna Loa; O_{SE}: Global Seasonal Ocean CO_2 Emission as Hypothesized by the WCRP; O_{SU}: Global Seasonal Ocean CO_2 uptake as Hypothesized by the WCRP; S_{LAND}: Global uptake of Atmospheric CO_2 through Land Sinks; S_{LUC}: Surface Area of Land use change; S_{OCEAN}: Global uptake of Atmospheric CO_2 through Ocean Sinks; S_{TOTAL}: $S_{LAND} + S_{OCEAN}$; E_{BDD}: Ocean Emission in Atmospheric CO_2 Related to the Biological Pump; U_{SIM}: Ocean Uptake in Atmospheric CO_2 caused by the Seasonal Ice Melt due to the inclination of the Earth Axis; U_{SLGHG}: Increase in Northern Pacific Ocean CO_2 uptake caused by Short Lived Greenhouse Gas Accumulation

Introduction

Efforts at understanding what drives Earth's climate date from the era of enlightenment when Herschel counted sunspots to predict temperature fluctuations [1]. Such early scientists are presented today as giants on whose shoulders we stand, but, in retrospect, science history narrows down earlier discoveries to the studies that are seemingly validating present day views while neglecting others. These neglected studies will be newly braided here into a pollutant driven climate model for System Earth which would have been

impossible without the wealth of data that a CO_2 driven model has generated for us.

Early considerations

The work of Foote represent such an early discovery [2]. Foote, referring to carbonic acid gas, concluded that "an atmosphere of that gas would give our Earth a high temperature". This is incontestably true, but a rapid evaluation of her work (Appendix 1, Figure 1) demonstrates that damp air (78% N_2 ± 20% O_2 ± 1% H_2O, and 1% of other gases, at the time comprising 0.028% CO_2) is as sensitive to solar irradiance as pure carbonic acid gas (100% CO_2).

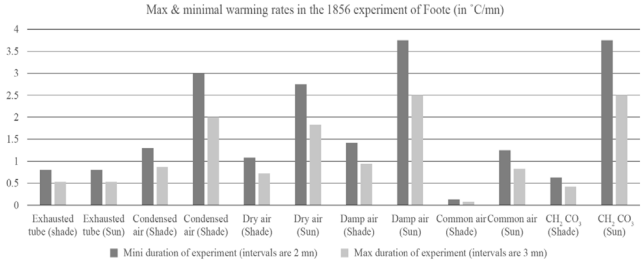

Figure 1: Example of erroneous historical validation of the CO_2 driven climate model for system earth. Visualization of the table of Foote where her error margin is highlighted as two colours because she measured temperature after 2 or 3 minutes. Some experiments were shorter than other ones and this analysis gives the rates of change for identical duration and identical measuring intervals. It is not possible to evaluate how damp her damp air was. Moreover, it seems difficult to obtain 100% pure carbonic acid gas as it is very unstable.

Tyndall, who repeated Foote's experiments, found that the most important GreenHouse Gas (GHG) was water vapour [3, 4]. Arrhenius, who tried to quantify how much of infrared (heat) radiation is captured by Carbonic Acid Gas (CO_2) and water vapour in Earth's atmosphere, did not rule out water vapour as GHG, but found CO_2 to be more effective [5]. The clustering analysis of the data from his table II illustrates that the absorption coefficients for CO_2 and water vapour (Appendix 2) did not differ significantly.

Arrhenius had dispatched De Marchi's hypothesis that water vapour is the main climate driver on Earth, because it required water vapour saturations beyond 100% [5,6]. We know now that condensation or crystallisation clouds represent saturation beyond 100% humidity as particulates function as either Condensation Cloud Nuclei (CCN) or as Ice Nucleating Particles (INP).

Particulates (CCN's or INP's) had made their appearance in the scientific perception when the Krakatau explosion of 1883 gave a wide global atmospheric belt of sky haze in the lower latitudes at altitudes well beyond the tropopause [7,8]. The explosion had resulted in an unmistakable temperature drop which was explained by the volcanic haze reducing solar irradiation [9].

Croll's hypothesis about glacial epochs following orbital forcing was also dispatched by Arrhenius who argued that obliquity causes identical temperatures on both hemispheres [10].

While carbonic acid, water vapour, particulates and the Milankovitch cycles had been hypothesized to contribute to our present day climate, it is relevant here to understand how carbon dioxide was found to represent the chief global temperature driver.

More recent developments

Evidence with respect to the warming effect of GHG followed from the "faint sun paradox" [11]. Atmospheric nitrogen compounds were expected to explain the high temperatures allowing for water to be liquid under the low solar radiation that a young sun would represent. Later, these GHG were preferred to be CO_2 as "CO_2 at high concentrations could have performed a similar function as could other polyatomic gases" [12].

By 1965 it was textbook knowledge that water vapour, carbon dioxide and ozone absorb outgoing radiation in the critical part of the light spectrum but only CO_2 was found to cause global warming (Figure 2) [13]. This focus may have followed from the "U.S. Standard Atmosphere of 1962" which approaches the atmosphere as composed of ideal air devoid of water vapour and dust. But instruments continuously registering particle concentrations at high altitude were already testifying to a scientific interest under less ideal conditions and when air transport moved to stratospheric altitude it caused scientific concern with respect to its climatic effect [14]. This gap in academic knowledge on aerosols had possibly developed due to the cold war [15].

Various early governmental reports predicted an increase in temperature of 3°C for a doubling of the atmospheric CO_2 concentration [16,17]. The 1983 report did state that "there does not appear to have been a significant long-term increase in the aerosol level in remote regions of the globe other than possibly the Arctic. One cannot even conclude that possible future anthropogenic changes in aerosol loading would produce worldwide heating or cooling, although carbon-containing Arctic aerosols definitely causes local atmospheric heating."

In the meantime the tropospheric ozone concentration increase in the northern hemisphere was found to stem from photochemical reactions with pollutants emitted by high-flying aircraft [18]. The properties of ozone as a GHG were not highlighted, in spite of the 1983 report where tropospheric ozone and water vapour were shown to strongly influence surface temperature changes (table 4.1).

The use of water has tripled since the 1960s and its industrial use has at least quadrupled but water isn't considered in terms of global temperature. Agriculture does raise concern because daytime cooling from irrigation is overshadowed by nocturnal warming from cloud cover [19, 20]. Industrial cooling causes water to leave the earth surface as hot damp polluted air that rises rapidly to stratospheric altitudes. These emissions form and pollute both condensation and ice clouds (cirrus), but were not highlighted in terms of climate drivers. So, in spite of a broad spectrum of known potential climate drivers, earliest efforts, as we will see below, focussed on CO_2.

Gaia hypothesis

In 1966, the oil industry appointed Lovelock to study a geotechnically enhanced biological pump that would draw down atmospheric CO_2 back into the oceans. This symptom-control-driven science led to the first steps at improving our understanding of System Earth but left us with the thought that marine algal blooms instead of taking up oceanic CO_2 take up atmospheric CO_2 [21].

By 1974, Lovelock and Margulis had introduced "life" (photosynthesis) as a geological force capable of stabilizing the early atmospheric temperature to the levels we have today. This is the Gaia hypothesis, requiring the seeding of condensation clouds with dimethyl sulphides to brighten clouds [12, 21]. Ayers and Cainey tried to quantify how algal blooms provide a feedback loop between life, marine cloud seeding, temperature, and carbon dioxide concentrations, but without success. Later, it was found that, apart from sulphides, numerous other particulates played a role as CCN [22, 23]. Besides, the Gaia model causing homeostasis was inconsistent with the Pleistocene climate cycle characterized by

regular temperature and atmospheric CO_2 concentration fluctuations.

The role of ozone

When the first hole in the ozone layer was discovered above Antarctica, the focus of the scientific community shifted to the short-term health implications of ultraviolet radiation while neglecting the climate issues related to the ozone depletion in the stratosphere [24-26]. In 1990 Yung had already understood that atmospheric CO_2 concentration is regulated by the oceans temperature and demonstrated that sulphates react with ozone. Later, it was demonstrated that black carbon aerosol (BCA) can carry nitric acid (HNO_3) and nitrogen dioxide (NO_2) and will react with stratospheric ozone converting it to oxygen [27,28]. These forgotten insights were 'rediscovered' later on [29-33]. They are the foundation for the present contribution.

From a broad set of possibilities to CO_2

By the end of the last century the first 1990 International Panel on Climate Change (IPCC) request for funding its international research was presented to the United Nations by stating upfront: "We are certain: there is a natural greenhouse effect which already keeps the Earth warmer than it would otherwise be; emissions resulting from human activities are substantially increasing the atmospheric concentrations of the GHG: carbon dioxide, methane, chlorofluorocarbons (CFCs) and nitrous oxide [34]. These increases will enhance the greenhouse effect, resulting on average in an additional warming of the Earth's surface. The main GHG, water vapour, will increase in response to global warming and further enhance it. The size of this warming is broadly consistent with predictions of climate models, but it is also of the same magnitude as natural climate variability". Simultaneously a NASA research team found that fire generated aerosols enhance solar ultraviolet radiation through ozone depletion [35]. This placed the ozone-hole in a short-term health context, neglecting the long-term climate context. Ozone had left the scientific arena as a potential climate driver.

The role of CO_2

A hypothetical backbone of a fully CO_2-driven System Earth made its public appearance in 2007 as the Global Carbon Budget (GCB) where the atmospheric accumulation of CO_2 was calculated as anthropogenic emission minus ocean uptake plus an unidentified sink [36]. The atmospheric increase in CO_2 concentration was recorded in the Keeling curve, the industrial emission was known, the required ocean sink had been established, but the unidentified sink was awaiting its discovery [37]. This was provided for a little later and by 2016, the GCB had fully developed into the Global Carbon Equation (GCE) [38,39]. The later states that the atmospheric increase in CO_2 (G_{ATM}), as recorded by the National Ocean and Atmospheric Administration (NOAA) at Mauna Loa reflects what CO_2 remains in the atmosphere after ocean (S_{OCEAN}) and land sinks (S_{LAND}) took up the bulk of the industrially (E_{FOS}) and agriculturally (E_{LUC}) emitted CO_2. Mathematically it is expressed in the following way:

$$(E_{FOS})+(E_{LUC})=(S_{OCEAN})+(S_{LAND})+(G_{ATM}) \quad (0)$$

This equation is the backbone of most climate models [40]. Simultaneously, ozone depletion was considered by another UN funded organization, the UN Environment program that developed the Montreal Protocol, in order to gain control over the industrial production of chlorofluorocarbons (CFC). The focus on CFC's is worrisome as the radical molecules which destroy ozone in the troposphere and the stratosphere are ubiquitously present and come with industrial pollutants [41,42].

The role of aerosols

In the IPCC model of 2022, clouds are presented as a diffuse shield. This representation does not do justice to water, which, at the pressures and temperatures related to the mass of our planet, is near its triple point [43]. This means that small pressure and temperature changes result in shifts in its phase causing our planet to be protected by a double shield. The external solid shield at the boundary of the troposphere and the stratosphere is composed of featherlike solid ice (cirrus) clouds. The internal shield consists of condensation clouds (stratus, stratocumulus or cumulonimbus clouds), that occupy the troposphere. Both cloud layers behave differently. While the ice clouds are part of the lower current of the stratospheric Brewer Dobson circulation cell and flow toward the poles of the hemispheric winter, the condensation clouds are confined to three climate cells (the Hadley, Ferrel and Polar cells) [44,45].

Both, cloud type and density, are determined by the availability of water and particulates. Water vapour, comprising 1%-3% of the tropospheric gases, isn't limiting the formation of clouds. It is the altitudinal distribution of the particulates that determines wat cloud type will be formed: At low altitudes particulates and aerosols from condensation clouds and higher up they form ice clouds.

The role of particulates as CCN's or INP's in Earth's albedo remained in the focus of the IPCC starting 1997, but also in their latest report from 2023 where they endorsed the view that direct negative forcing of aerosols masks part of the GHG global warming [46-48]. However, in 2023, global climate models still fail at accounting for the role of dust concentration [49]. Indeed, it appears that aerosol emissions that seed condensation clouds caused regional dimming, but cannot explain the subsequent brightening trends [50]. Similar types of uncertainties were found for aerosol/ice cloud interactions, where albedo effects can be established regionally but can't be repeated in global climate models [51].

It is surprising in this respect how the albedo was considered only, because Liss and Lovelock had concluded that a cocktail of gases and aerosols was reacting with ozone. This is highly relevant as ozone depletion cools the stratosphere but warms the troposphere [52, 53]. Moreover the photolysis of ozone is often exothermic while winter accumulation of ozone in the Arctic can cause seasonal warming [54,55].

An aerosol-driven System Earth is supported by our knowledge from earth history. Indeed, dust (loess) typically characterizes glacial maxima of the Antarctic Pleistocene, while charcoal peaks appear in their tropics [56,57]. Similarly midlatitudes underwent wildfire intensification during the past eight glacial maxima, the intensity of which has been found to be inversely correlated with global atmospheric CO_2 concentrations [58].

Natural forest fires do not only produce pollutants such as SO_2 and NO_x, but their high-temperature carries particulates to the tropopause where the lower current of the stratospheric Brewer Dobson cell carries them to the pole of the hemispheric winter where they can be seen to cause the arctic heat anomaly. Indeed, nitrogen compounds are found to cause the accumulation of the short lived greenhouse gas ozone [59-62].

That ozone can be seen to accumulate in the troposphere of the polar winter night but gets depleted with the return of the light in spring. Ozone also gets depleted in the lower stratosphere [63,64]. The cycle of ozone, consequently, requires further scrutiny as ozone accumulation in the troposphere can cause tropospheric warming, while stratospheric ozone depletion results in tropospheric warming [33].

A role for the arctic heat anomaly

The short lived GHG ozone has been reported to give heat accumulation in the troposphere and to result in aberrant polar vortex

behavior. The outer rim of the polar vortex forms the jet stream. Lower atmospheric warming, the northern jet-stream intensity and sea-ice cover in the Arctic are correlated [53,65]. During the last Pleistocene climate cycle there is evidence for the dry trade wind and wet storm periods on Hawaii to be related to the intensity of this same northern jet stream [66]. Reconstructions of the climate in the past provide therefore evidence that not only the Milankovitch cycles force climate on Earth, but so do aerosols. Even the frequency of the El Niño events in South America can thus be explained [67].

Despite the 1987 UN Montreal Protocol that appeared to restore the ozone hole above the Antarctic, a second hole appeared in the ozone layer above the Arctic in 2020 [64]. Moreover, the annual mean Arctic temperature amplification has become increasingly clear [68]. So time has come to determine whether the sum of all emitted pollutants (aerosols, dust, charcoal, sea spray) rather than dimming solar radiation, induces arctic warming through ozone and pollutant accumulation and global warming through its depletion in the stratosphere.

A new hypothesis for the carbon cycle

In the following it will be demonstrated that seasonal ocean emission (O_{SE}) and seasonal uptake (O_{SU}), as defined by the GCE, in contradiction to the existing assumptions that the two are equal, do not even out [69].

Also, the error margins for the land sinks (S_{LAND}) and the emission from land use change (E_{LUC}) will be demonstrated to be too large to build upon [70,71]. Moreover the relation between E_{LUC} and atmospheric CO_2 growth (G_{ATM}) will be shown to be the contrary of what the World Climate Research Program (WCRP) has expected and still expects [39,40]. It will be made admissible that pollutants, rather than CO_2 emissions, cause global warming and in the wake of this global warming, ocean degassing of *i.e.* CO_2.

This new pollutant driven model for System Earth will be substantiated by reconstructing the Keeling curve as the sum of six functions determining the G_{ATM} as recorded by NOAA in the Northern Pacific Ocean, four of which are proportional to industrial pollutant emission. This new interpretation of the Keeling curve will be shown to be consistent with a vegetation and stratospheric ozone driven Pleistocene climate cycle.

Material and Methods

Data sets

The data of Foote and Arrhenius were used respectively for a histogram and a principle components analysis in PAST as offered in Hammer et al. [72] (Table 2 and Appendices 1,2).

Analysis of hourly daily and monthly averages of the G_{ATM} for Mauna Loa and the South Pole are freely available online [73] (Appendices 3-6).

The industrial emissions from fossil fuels (E_{FOS}) came from Liu et al [32] (Figure 1). The emission caused by land use change (E_{LUC}) is also made available by the website of the Carbon Brief [71]. The uptake in atmospheric CO_2 by land sinks (S_{LAND}) was taken from Gasser et al. [70]. The surface of land use change was taken from Winkler et al. [74]. The ocean sink (S_{OCEAN}) values were from Bennington et al [75]. Friedlingstein et al. was used for the transfer from ppm CO_2 to Gigaton (Gt) carbon. Pollutant concentrations in the atmosphere from various atmospheric chemistry models over time were found in Griffiths et al. [76] (Appendix 7).

Two of these pollutant cocktails were compared to what Friedlingstein et al. consider industrial emission ($IE=E_{FOS}+E_{LUC}$). The cocktails are the UKESM1-0-LL model that includes Volatile Organic Carbons (VOC) and the CESM2-WACCM model including Secondary Organic Aerosols (SOA) [76] (Table 1). The highest determination coefficient (R^2) and the lowest probabilities (p), under the assumption that industrial emission ($IE=E_{FOS}+E_{LUC}$) is a proxy for atmospheric chemistry, were used to establish that the UKESM1 model reflects industrial emission best Table 1).

X axis	Y axis	R^2:	p:	Equation
IE	UKESM1	0.97837	1.64E-42	$Y=-11.36\ x^2 + 227.5x-262.8$
UKESM1	CESM2	0.95461	1.16E-33	$Y=0.0003063\ x^2 + 1.173\ x-226.8$
IE	CESM2	0.9511	9.05E-37	$Y=-9.12\ x^2 + 179.2\ x-310.6$

Table 1: Comparison between pollutant production and industrial CO_2 emission. Two functions modelling the net chemical production minus loss of O_3, UKESM1-0-LL with a focus on Volatile Organic Carbons (VOC), and CESM2-WACCM with a focus on secondary organic aerosols as shown in Griffiths et al. are compared to the sum of fossils fuels (E_{FOS}) plus the emission caused by land use change (E_{LUC}) considered in the GCE to reflect industrial emission ($IE=(E_{FOS}) + (E_{LUC})$).

The impact of pollutants and industrial CO_2 compared

The polynomial regression analyses of Hammer et al. were used to compare the determination coefficients (R^2) and probabilities (p) between the pollutants and the yearly ocean behaviour at Mauna Loa, *viz*. yearly atmospheric CO_2 increase (ML_{YI}), yearly atmospheric CO_2 decrease (ML_{YD}) and their difference, being the yearly growth of the atmospheric CO_2 (G_{ATM}) [72]. The number of examined polynomial functions was reduced to the 46 most relevant ones by ordering them according to best probability (Appendix 8).

Two methods to calculate atmospheric CO_2 growth

Two calculation methods for G_{ATM} are compared in here, *viz*. the method followed by the WCRP and present method (Appendix 3, Figure 2) [42]. The WCRP evened out seasonality in the atmospheric CO_2 growth ($G_{ATM-WCRP}$) following Ballantyne et al. [69].

In the present contribution, G_{ATM} is calculated by subtracting the yearly atmospheric CO_2 decrease/ocean uptake (ML_{YD}) from the yearly atmospheric CO_2 increase/ocean emission (ML_{YI}) from the consecutive period ($G_{ATM-Here}$) (Figure 2).

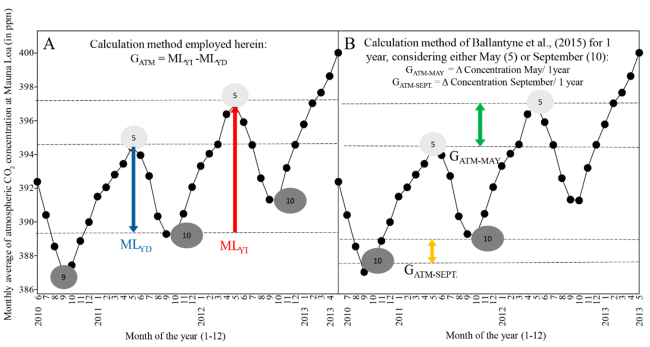

Figure 2: Details of the Keeling illustrating two ways to calculate the yearly atmospheric growth (G_{ATM}). **Note:** A. Method used here in: $G_{ATM-Here}=ML_{YI}-ML_{YD}$. B. Method used by the WCRP: $G_{ATM-WCRP}=\Delta C/\Delta t$.

This was done on the basis of the selection of highest and lowest emission month of each year between 1961 and 2019 as offered by the NOAA. The value of the yearly atmospheric decrease/ocean uptake in CO_2 (ML_{YD}) was calculated by subtracting the lowest monthly atmospheric CO_2 concentration from that year from the value of the highest monthly CO_2 concentration preceding it.

The yearly atmospheric CO_2 increase/ocean emission (ML_{YI}) was obtained by subtracting the lowest monthly values in atmospheric CO_2 concentration from the highest monthly concentration following it (Appendix 3,9).

The $G_{ATM\text{-}Here}$ and the $G_{ATM\text{-}WCRP}$ were calculated for one and for three years (Appendix 9). Box plots of $G_{ATM\text{-}Here}$ and the $G_{ATM\text{-}WCRP}$ were compared with the statistical PAST program [72]. The difference between the various calculations of G_{ATM} was also evaluated by calculating their percentage error as follows:

Percentage error=averaged G_{ATM}–actual G_{ATM} (of $G_{ATM\text{-}Here}$ or $G_{ATM\text{-}WCRP}$)/actual G_{ATM} x 100.

Reconstruction of the Keeling curve

Regional seasonality: Hakkarainen et al. showed that seasonality approaches symmetry in the high latitudes of the southern hemisphere, unlike the northern hemisphere where it clearly is asymmetrical [77].

This symmetry was hypothesized here to reflect the near absence of industrial bias to the seasonal warming or cooling in the Antarctic. We reproduced such a yearly emission diagram here for the randomly chosen period of 1990 to 1996 using the monthly data sets provided by NOAA, for both Mauna Loa and the South Pole (Figure 3) [78].

Approximation of seasonality on both hemispheres: A second-order regression analysis of the monthly atmospheric CO_2 as recorded by the NOAA on Antarctica (Appendix 5) served to establish the global ocean emission, expected to be free of seasonality (Figure 4).

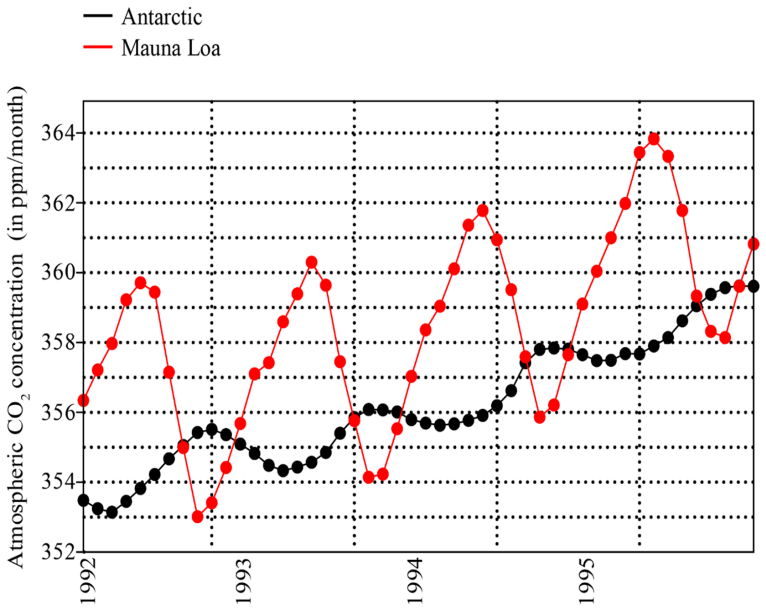

Figure 3: Visualization of the difference in yearly amplitude between the atmospheric CO_2 concentrations in different geographical localities for the randomly chosen 1992-1996 period. (a) Mauna Loa (red line), (b) South Pole (black line). The data are from NOAA (Appendix 5).

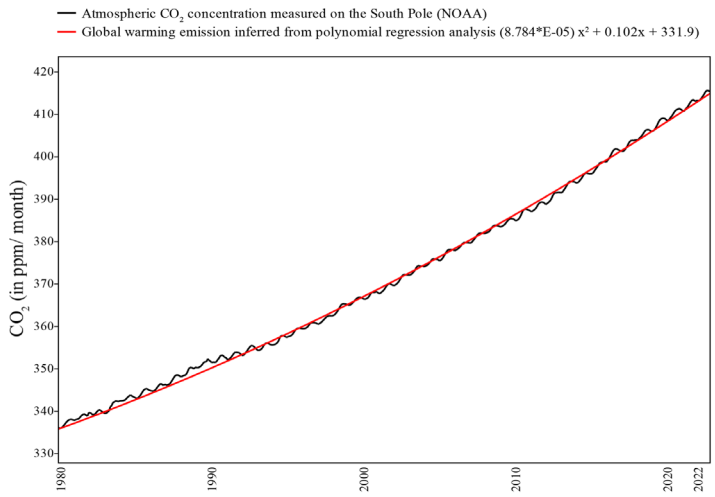

Figure 4: Polynomial function drawn through the monthly atmospheric CO_2 concentrations as recorded by NOAA on the South Pole between 1980 and 2022 [79].

This gave a function of $y=8.784^{*}x^{2}E^{-05} + 102^{*}x + 331.9$.

This function serves to establish the average seasonal amplitude in atmospheric CO_2 emission of the south pole by subtracting the monthly average from the mean determined by the function $y=8.784^{*}E^{-05}\ x^{2}+ 102^{*}x + 331.9$

The maximum amplitude of these monthly excursions from the regression line for the month of weakest (March) and strongest atmospheric CO_2 concentrations (December) were summed up, averaged and divided by two. This gave an approximation of the seasonal southern hemispheric positive and negative atmospheric CO_2 excursions from the global ocean emission. It was varying between 0.25 to -0.25 ppm (see Appendix 6). Because continents occupy approximately 2 x as much surface on the northern hemisphere as on the southern hemisphere, the seasonality was expected to vary between 0.5 to -0.5 ppm on the northern hemisphere.

Yearly obliquity and industrial uptake: The function of yearly ocean CO_2 uptake for the Northern Pacific Ocean was made inversely proportional to the sea ice extant as found in Yulin et al. [79]. The seasonal uptake of maximally -0.5 ppm was made proportional to the duration of the melting period [79]. The remaining yearly uptake excursion of approximately 4.5 ppm was constructed with the expectation that the pollutant emission causes the arctic heat anomaly and enhances the arctic ice melt. Therefore, it was made proportional to both, the duration of the melting period and the UKESM1 curve (Appendix 10).

Yearly obliquity and industrial emission: The seasonal CO_2 emission was made equal to the yearly sum of the yearly uptake in CO_2 and proportional to the average day length at 60 degrees North (Appendix 11).

The function of yearly industrial pollutants enhanced ocean CO_2 emission for the northern hemisphere was constructed with the expectation that the pollutant emission is proportional to the heat produced by pollutants in the Arctic, which heat is taken up by the oceans resulting in the zone of CO_2 emission in the northern hemisphere as depicted by Hakkarainen et al. [77]. This pollutant induced CO_2 emission was spread in a yearly returning series of percentages established in comparison to the CO_2 emission vague as observed in Hakkarainen et al. and proportional to the UKESM1 curve [76,77] (Appendix 10) (Figure 3).

Stationary and cumulative functions: The functions of seasonal and industrially driven hydrosphere warming and cooling were made stationary. For the seasonality of the CO_2 emission and uptake, this is self-explanatory, as they are driven by recurrent temperatures. For industrial pollutants this is explained through thermal energy being fully transformed into chemical energy.

Global warming proportional to pollutant emission: Also, part of the solar irradiance energy causes the air mass to be ascending in the troposphere. This ascending energy is expected to return to chemically energy when the stratospheric ozone layer gets depleted. The increase in solar radiation following from the stratospheric ozone depletion was made cumulative as the thickness of the ozone layer is transformed permanently. It was made proportional to the curve of the UKESM1 cocktail [76] (Appendix 10).

Estimating the impact of El Niño events: The biological pump is necessarily part of the chemical solubility pump. It is its dysfunction through El Niño events that are seen here to influence the carbon cycle, thus resulting in enhanced ocean CO_2 emission of approximately 0.3 ppm [80]. Such events last several months and are here spread from November to January. As we had about 12 El Niño events in the past 60 years and no change in its frequency could be found, this enhanced CO_2 emission was made to occur on 12/60-th of its intensity every year.

Comparing to the Keeling curve: The sum of all six functions (two seasonal, two seasonal-industrial, one biological and one stratospheric) represents the monthly atmospheric CO_2 concentration from 1961 to 2019, which was added to the atmospheric CO_2 concentration of January 1961. This result was compared with the monthly Keeling curve (Appendix 10) using a polynomial regression analysis.

Results

The atmospheric increase in CO_2 concentration was calculated as by the World Climate Research Program [40] ($G_{ATM\text{-}WCRP}$) for the months of strongest emission (from May to May) and lowest emission (from September to September) and were compared with box plots to the atmospheric increase in CO_2 concentration calculated in the present contribution ($G_{ATM\text{-}Here}$). This was done for a period of one year, as well as for the average over three years (Appendix 9). Although this seems just a simple difference in methodology, it reflects a fundamental difference in interpretation. While the $G_{ATM\text{-}Here}$ is considered to reflect ocean behaviour being seasonally influenced by industrial emission and stratospheric ozone depletion, $G_{ATM\text{-}WCRP}$ is believed to represent the yearly carbon equation, where seasonality is evened out because seasonal ocean CO_2 uptake is expected to be equal to seasonal CO_2 emission (Figure 5).

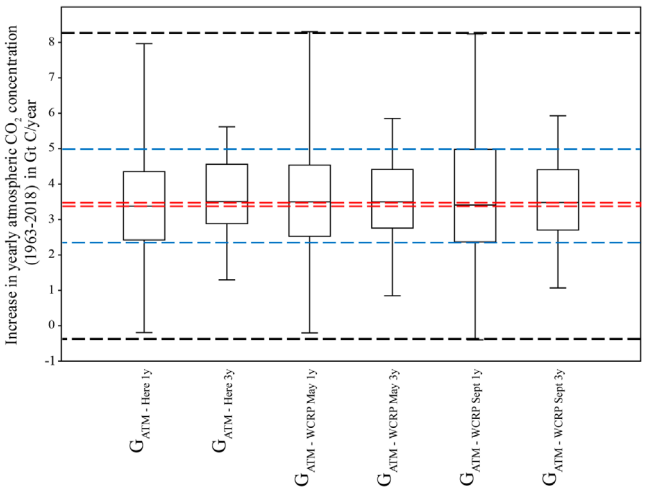

Figure 5: Box plots allowing for the comparison of six potential methods to calculate the atmospheric increase in CO_2 concentration. **Note:** $G_{ATM\text{-}Here}$ 1y: method used herein ($G_{ATM\text{-}Here}$ $1y=ML_{YI}\text{-}ML_{YD}$) for one year; $G_{ATM\text{-}Here}$ 3y: method used here in for the average of 3 years; $G_{ATM\text{-}WCRP}$ May 1y: method used by the W_{CRP} ($G_{ATM\text{-}WCRP}$ $1y=\Delta C/\Delta t$), from May to May of the former year; (d) $G_{ATM\text{-}WCRP}$ Sept 1y: method used by the W_{CRP} from September to September from the former year; $G_{ATM\text{-}WCRP}$ May 3y: method used from May to May of three years before; $G_{ATM\text{-}WCRP}$ Sept 3y: method used by the W_{CRP} from September to September from the three years before. Black dashed rectangle: largest spread; blue dashed rectangle: largest interquartile; red dashed rectangle: lowest and highest medians.

The comparison of the six methods to calculate G_{ATM} indicates that the method employed here ($G_{ATM\text{-}Here}$) gives the same results as for the methods used by the WCRP. Indeed:

- The median of $G_{ATM\text{-}here}$ as calculated here for a single year is slightly inferior to $G_{ATM\text{-}WCRP}$ for May and September (May 1y, Sept. 1y), while the median of $G_{ATM\text{-}Here}$ for three years is slightly larger than the $G_{ATM\text{-}WCRP}$ for September for three years but equal

to the other calculations of $G_{ATM\text{-}WCRP}$ for May and September.

- The interquartile range of $G_{ATM\text{-}WCRP}$ September 1 year is larger than all others, including both calculation methods for $G_{ATM\text{-}Here}$.
- The same is the case for the spreading of $G_{ATM\text{-}WCRP}$ September 1 year.

Moreover, the errors between the averages of all 6 calculation methods for the increase in atmospheric CO_2 concentration were also considered (Table 2). The largest error (-1.56 %) was obtained for the 3-year calculation of our $G_{ATM\text{-}Here}$, and the smallest (0,09 %) for the $G_{ATM\text{-}WCRP}$ from the World Climate Research Program for September for 1 year.

G_{ATM}	Error margin
$G_{ATM\text{-}WCRP\ Sept\ 3y}$	1.33
$G_{ATM\text{-}Here\ 1y}$	0.78
$G_{ATM\text{-}WCRP\ May\ 3y}$	0.38
$G_{ATM\text{-}WCRP\ Sept\ 1y}$	0.09
$G_{ATM\text{-}WCRP\ May\ 1y}$	-0.97
$G_{ATM\text{-}Here\ 3y}$	-1.56

Table 2: Comparison between the six calculation methods for atmospheric CO_2 growth. **Note:** Error margin for the average value for the atmospheric increase in CO_2 concentration (G_{ATM}) between 1963 and 2018 calculated as $G_{ATM\text{-}Here}=ML_{YI}-ML_{YD}$ for one or three years or as $G_{ATM\text{-}WCRP}=\Delta C/\Delta t$, when considering the month of strongest emission (May) and the month of weakest emission (September) for a period of one year and a period of 3 years.

It can consequently safely be said that the $G_{ATM\text{-}Here}$ calculated as yearly ocean CO_2 emission minus yearly ocean CO_2 uptake reproduces the $G_{ATM\text{-}WCRP}$ as calculated by the World Climate Research Program (WCRP) [40]. This means that the following is true.

$$G_{ATM\text{-}Here}=G_{ATM\text{-}WCRP} \quad (1)$$

Implications for the Global Carbon Equation

The Global Carbon Equation (GCE) states that the total industrially emitted CO_2 ($IE=E_{FOS}+E_{LUC}$) minus total up taken CO_2 ($S_{TOT}=S_{OCEAN}+S_{LAND}$) is equal to the atmospheric increase in CO_2 concentration (G_{ATM}), or:

$$IE-S_{TOT}=G_{ATM\text{-}WCRP} \quad (2)$$

As demonstrated above, $G_{ATM\text{-}WCRP}=G_{ATM\text{-}Here}=ML_{YI}-ML_{YD}$, this indicates that the GCE can also be expressed as:

$$IE-S_{TOT}=ML_{YI}-ML_{YD} \quad (3)$$

(Or)

$$(IE-S_{TOT})-(ML_{YI}-ML_{YD})=X \quad (4)$$

If the Global Carbon Equation is correct, then X=0. This is tested below with the box plots of the averages of this equation over time (Figure 6).

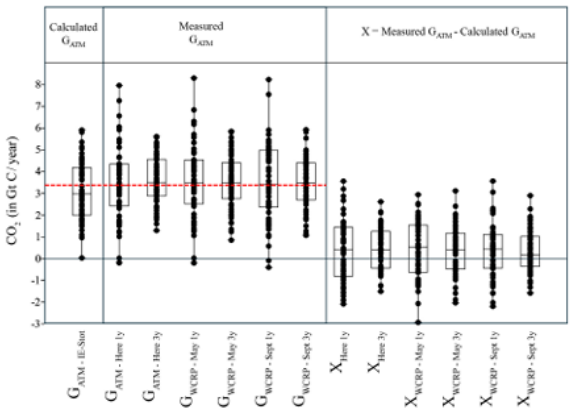

Figure 6: Superimposed box and jitter plots for equation (2). **Note:** G_{ATM} calculated as IE-STOT, as $G_{ATM\text{-}Here}$ ($=ML_{YI}-ML_{YD}$) for one and three year, measured as $G_{ATM\text{-}WCRP}=\Delta C/\Delta t$, for the month of May and September for one and three years, respectively; the difference X between the six calculations methods for G_{ATM} basisd on the measurements at Mauna Loa and G_{ATM} calculated as IE-S_{TOT}; red dashes line: Median of G_{ATM} as calculated here for one year.

In this box plot we see that X isn't equal to 0 and remains positive. Furthermore when comparing X, for instance, to the diurnal fluctuation recorded on the 28-th of July 2024 (>8 ppm CO_2 or >16 Gt C), these differences appear insignificant. But when taking the averages of all calculation methods of X (0,395 Gt C) and comparing it to the averages of the various parameters of the GCE (Table 3), it is clear that the imbalance X represent a high percentage of the atmospheric CO_2 sinks and sources thus indicating that these data are still too tentative to allow for the modelling of the GCE.

Sinks & sources of CO_2	Average (in Gt C/ year) from 1963 to 2018	% of the average X (0.395 Gt/year) of the various sinks and sources
S_{LAND}	2.18	18%
S_{OCEAN}	1.91	20%
E_{FOS}	5.97	6%
E_{LUC}	1.27	31%

Table 3: Analysis of average imbalance X in the GCE and the average value of the different members of the GCE. **Note:** The averaged values of all sinks and sources were calculated with Appendix 7. The average imbalance in the GCE of X was calculated as ((100 /Average of sinks & sources)*Average X).

In search of X

According to the WCRP [40] seasonal ocean CO_2 emission (O_{SE}) and seasonal ocean CO_2 uptake (O_{SU}) are equal and even out.

Also according to the WCRP the yearly CO_2 emission (ML_{YI}) is the industrial CO_2 emission (IE) plus the seasonal ocean CO_2 emission (O_{SE}). This can also be expressed as:

$$ML_{YI}=IE+O_{SE} \quad (5)$$

Still according to the WCRP [40], the yearly CO_2 uptake (ML_{YD}) is the total of the CO_2 sinks (S_{TOT}) plus the seasonal ocean CO_2 uptake (O_{SU}). This can be expressed as:

$$ML_{YD}=S_{TOT}+O_{SU} \quad (6)$$

As IE, S_{TOT}, ML_{YI} and ML_{YD} are known, O_{SU} and O_{SE} can be calculated (Appendix 12).

$$O_{SE}=ML_{YI}-IE \quad (7)$$

$$O_{SU}=ML_{YD}-S_{TOT} \quad (8)$$

The box plots of these yearly calculations indicate that the difference between the seasonal ocean emission (O_{SE}) and the seasonal ocean uptake (O_{SU}) is positive, significant and equal to X for a calculation using the $G_{ATM\text{-}Here}$ for one year (Figure 7). All other five calculation methods of X and G_{ATM} based on the data at Mauna Loa give similar results but are not shown here for practical reasons. This indicates within the approach to the GCE by WCRP the basal paradigm [69] (that O_{SE} and O_{SU} are equal and could be made to even out) is not true.

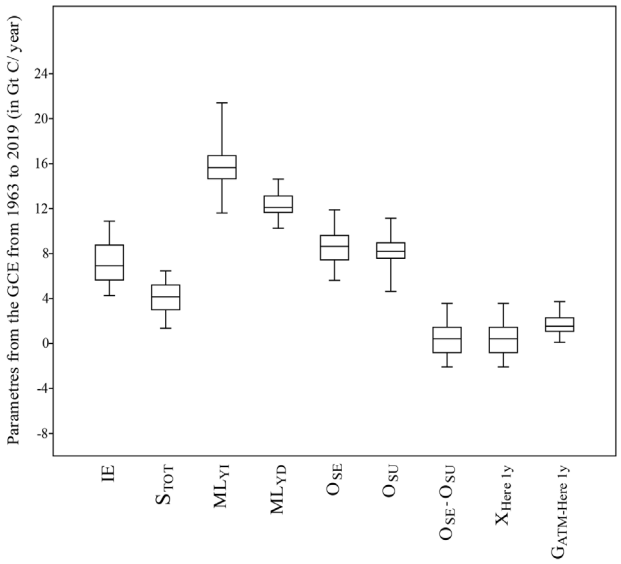

Figure 7: Box plots illustrating that X, the imbalance in the GCE, is positive and reflects the difference between seasonal ocean CO_2 emission and seasonal CO_2 uptake. **Note:** ML_{YI}: yearly atmospheric increase in CO_2, ML_{YD} yearly atmospheric decrease in CO_2, IE: Total of the industrial emission ($E_{FOS}+E_{LUC}$), S_{TOT}: total of the CO_2 sinks ($S_{OCEAN}+S_{LAND}$), O_{SE}: Seasonal Ocean Emission, O_{SU}: Seasonal Ocean CO_2 uptake, G_{ATM}: $G_{ATM\text{-}Here}$ 1y.

X compared to land sinks and land use change over time

Quite obviously, the disbalance X, within the GCE is mild, but nonetheless about 18 % of the average yearly atmospheric CO_2 uptake through land sinks and even 31 % of the emission through land use change [70,71].

The imbalance in the GCE not only represent a high percentage of the yearly land sinks and sources, but large error margins were also said to exist in the data sets from the original registrations [70]. It is therefore relevant here to review the relation between atmospheric CO_2 growth (G_{ATM}) and land use change (E_{LUC}) or land sinks (S_{LAND}) (Figure 8).

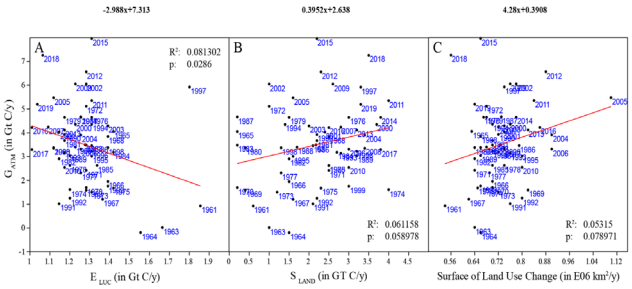

Figure 8: Counterintuitive relation between atmospheric CO_2 growth (G_{ATM}) and land CO_2 sinks and sources. **Note:** A) Correlation between atmospheric growth (G_{ATM}) and land use change emission in CO_2 (E_{LUC}). B) Correlation between atmospheric growth (G_{ATM}) and CO_2 land sinks (S_{LAND}). C) Correlation between atmospheric growth (G_{ATM}) and the surface area of land use change (S_{LUC}).

A very clear correlation between the development of the sinks and source over time and the G_{ATM} was not expected here, but the statistical analysis between the three should have confirmed the nature of the correlation hypothesized by the WCRP. This is not the case. The CO_2 emission from land use change (E_{LUC}) correlates negatively with the atmospheric CO_2 growth (G_{ATM}). This is confirmed by the positive correlation between CO_2 land sink uptake (S_{LAND}) and the same atmospheric CO_2 growth (G_{ATM}). The determination coefficients are weak, but the probabilities are relevant. Consequently the initial hypothesis that agriculture causes CO_2 emission and that land sinks result in CO_2 uptake is either unproven or incorrect. This paradox will be explained below and in the discussion section, but here we focus on the implications of present results for the GCE.

The relation established by the WCRP for the GCE between industrial CO_2 emission and ocean and land CO_2 sinks is expressed in (9):

$$(E_{FOS}+E_{LUC})-(S_{OCEAN}+S_{LAND})=G_{ATM} \quad (9)$$

In our statistical analysis (Fig 8) land use change CO_2 emission (E_{LUC}) decreases as atmospheric CO_2 growth (G_{ATM}) increases, while land sinks CO_2 uptake (S_{LAND}) increase as G_{ATM} increases. It is consequently diametrically opposed to the original GCE. Because in Figure 8 S_{LAND} appears to emit CO_2, while E_{LUC} appears to take it up, in spite of the statistics being weak, they rather reflect a GCE expressed as: "assuming seasonality evens out, all emitted CO_2 (E_{FOS} +S_{LAND}) minus all up taken CO_2 (S_{OCEAN} +E_{LUC}) reflect atmospheric CO_2 growth (G_{ATM})" which in mathematical terms looks like the following equation (10):

$$(E_{FOS}+S_{LAND})-(S_{OCEAN}+E_{LUC})=G_{ATM} \quad (10)$$

This paradox is elucidated when comparing the surface of land use change (S_{LUC}) to G_{ATM} (Figure 8 C). It is a positive correlation and indicates that something other than E_{LUC} is causing atmospheric CO_2 growth (G_{ATM}) and that this new factor correlates to the surface of land use change (S_{LUC}).

As was explained in the introduction, volatile organic carbon, water vapour, black carbon, aerosols and pollutants play a part in the mitigation of cooling at the glacial maximum; here we hypothesise that the surface of land use change is a proxy for the emission of such pollutants.

A new hypothesis

Thus we can deduce that the Global Carbon Equation stating that atmospheric CO_2 growth (G_{ATM}) represent the difference between Industrial Emission (IE) and natural sinks (S_{TOT}) is debatable because it

- Leans too heavily on tentative estimates for S_{LAND} and E_{LUC};
- Represent a debatable hypothesis on the relation between S_{LAND} and E_{LUC} and G_{ATM};
- Requires that, within the GCE, seasonality is evens out, which is not the case.

From here on, the GCE is abandoned and the new hypothesis that G_{ATM} simply reflects the difference between ocean emitted and up taken CO_2, is explored.

Implications of the new hypothesis

The chief implication of this new interpretation of G_{ATM} as ocean generated is that, if ocean emission (ML_{YI}) is superior to ocean uptake (ML_{YD}), this positive imbalance can only be explained by the oceans releasing more CO_2 than that they take up. This means that the oceans are not taking up an excess in industrial CO_2 and that industrial CO_2 emission is not or hardly perceived in the troposphere. As industrial CO_2 isn't clearly perceived in the troposphere it doesn't accumulate there and consequently industrial CO_2 can't cause global warming.

In the absence of CO_2 as the chief driver for global warming and taking into account that the surface of land use change, being a proxy for pollutant emission, plays a part in the atmospheric CO_2 increase (Figure 8), it will be demonstrated in the following that pollutants can, indeed, induce the warming that causes oceans to release their gases.

Having reviewed, in the introduction, the diversity in potential climate drivers, we then build on Liss and Lovelock [52] who predicted that it was "… perhaps naïve to think that one gas acting alone (e.g. dimethyl sulphide) is responsible for particle formation; it is much more likely that a cocktail is involved. Many of these gases also play potentially important roles in air quality, particularly halogens in ozone destruction".

Comparing pollutant emission and ocean behaviour

UKESM1 being the pollutant cocktail that compares best with industrial CO_2 emission (Table 1), the relation between yearly ocean emission (ML_{YI}), the yearly ocean uptake (ML_{YD}) and their difference (G_{ATM}) are compared here (Table 4).

X-axis	Y-axis	R^2	p:	Equation
UKESM1	ML_{YI}	0.5442	3.96 E^{-11}	0.0116 x + 7.537
UKESM1	G_{ATM}	0.40494	7.94 E^{-08}	0.00835 x - 2.982
UKESM1	ML_{YD}	0.09629	1.78 E^{-02}	0.002422 x + 10.52

Table 4: Comparison between pollutant emission and Northern Pacific Ocean behaviour. **Note:** The determination coefficients (R^2) and probabilities of not being correlated (p) from a polynomial regression analysis between of pollutants (UKESM1) to the yearly ocean CO_2 emission (ML_{YI}), yearly ocean uptake (ML_{YD}) and their difference (G_{ATM}) are shown here.

The R^2 values in Table 4 indicate that pollutants determine 54% of the yearly ocean CO_2 emission (ML_{YI}), 9 % of the yearly ocean CO_2 uptake (ML_{YD}) and 40 % of the tropospheric increase in CO_2 concentration (G_{ATM}). This indicates that industrial pollutant emission influences both ocean CO_2 uptake as ocean CO_2 emission but the emission more than the uptake.

Ocean behaviour over time

When comparing monthly and yearly ocean uptake and emission over time it appears, indeed, that both their intensities increased over time. While ocean uptake, on a monthly basis, is more intense than ocean emission, the duration of ocean emission is longer than the duration of ocean uptake (Figure 9). This results in a near systematic dominance of yearly ocean CO_2 emission over yearly uptake. This intensity and duration analysis also indicates that for the period of 1961 to 2019, the duration in month of ocean uptake decreased in favour of ocean emission.

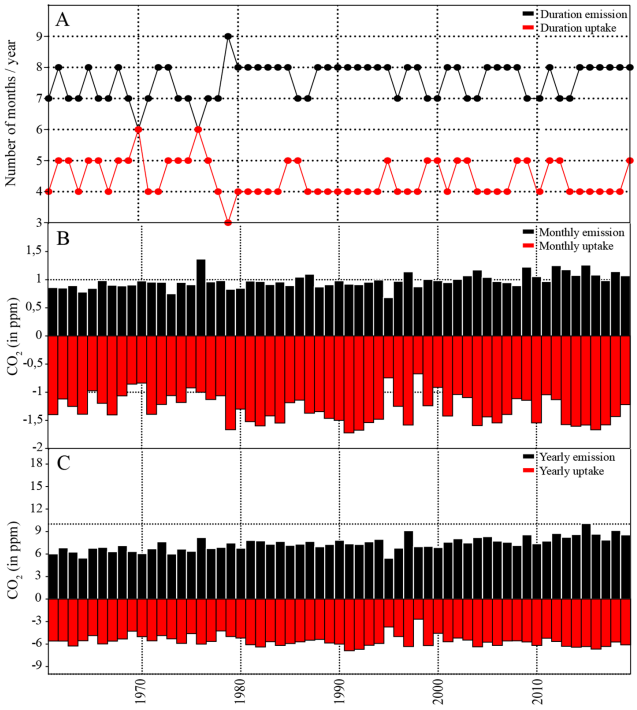

Figure 9: Ocean CO_2 uptake and emission. **Note:** A. Duration of ocean CO_2 uptake (red) and CO_2 emission (black) compared. B. Monthly ocean CO_2 uptake (red) and monthly ocean CO_2 emission (black) compared. C. Yearly ocean CO_2 uptake (red) and yearly ocean CO_2 emission (black) compared.

Interpretation

A heat anomaly stemming from the high latitudes: Seasonal CO_2 ocean emission, appears in the early spring in the high latitudes of the Northern Pacific, moves gradually towards the low latitudes until June, after which it disperses in southern direction [81].

This emission wave is interpreted here to result from heat for which we invoke the Le Chatelier principle. It states that changes in temperature, pressure, volume, or internal concentration of a solute, each and all can shift the equilibrium state of the solute [82]. The oceans are a chemical solute with a constant pressure and volume. Hence, only temperature will shift the internal concentration of its solutes.

Pollutants causing the arctic heat anomaly: Tropospheric

ozone is formed in the presence of pollutants and lightning [83]. It accumulates at the poles because it has a photochemical reaction with volatile organic carbons [84].

Because the reactions are photochemical ozone accumulates in the Arctic winter night and only starts reacting when light returns in spring. The ozone enriched air mass becomes relatively warm because the reactions with ozone can be exothermic and ozone is a Short Lived GHG. These processes are interpreted as responsible for the Artic heat anomaly.

Sources of pollutants reaching the Arctic: As explained in the introduction, natural forest fires produce massive quantities of SO_2 and other pollutants like NO_x or NH_3 [59,60]. Both forest fires and the burning of coals generate soot particles found in the atmosphere [85]. Smoke from wildfires also contributes to particulates in the stratosphere as recent wildfires are reported to have brought smoke into the stratosphere of Canada, United States and Australia [86-89].

All these fires reflect complete and incomplete combustion of organic molecules forming pollutants as for instance alkenes. Alkenes occur in the natural system in cuticular waxes of plants [90]. Such molecules also contribute to (green) fossil fuels, rubbers (natural and industrial), and to plastics [91]. Hence, fire (natural and industrial) injects pollutants in the troposphere. Elevated temperatures or simple air transport bring the particulates to the tropopause where they form INP to the cirrus clouds [92-93]. Polluted cirrus clouds concentrate yearly in each hemispheric winter pole driven by the lower current of the Brewer Dobson stratospheric circulation cell [44].

The arctic heat anomaly causing ocean emission: Aleutian low events from the Northern Pacific Ocean are reported to respond to anthropogenic forcing [94]. The Self-lofting CHemically reactive Arctic Winter accumulated Air Bubble (SCHWAB) described above, is considered here to cause such events but also the Hawaiian High as can be inferred from Holocene Vegetation fluctuations on Hawaii, thus intensifying the storms that incorporate heat into the ocean by deepening the thermocline [95]. As the thermocline deepens, the ocean warms and releases its gases, amongst other CO_2. These gases come to enrich the ascending air mass in the upwards air currents from the Hadley cell, which we can follow thanks to the science community's focus on CO_2 [96]. This air mass appears in the Arctic high latitudes/ low altitudes and escapes to the stratosphere in the low latitudes/high altitudes [96]. The amount of pollutants reaching the high latitudes is considered here to determine the intensity of the Arctic heat anomaly and the size of the SCHWAB.

Ocean emission causing stratospheric ozone depletion: Part of the heat generated by the SCHWAB gets incorporated in the ocean through storms, lowering the thermocline which results in the emission of a broad spectrum of ocean gases as illustrated here [95-97] (Table 5).

Gas type	Concentration in water at 0˚C	Concentration in water at 60˚C	Solubility indicator ((concentration at 0˚C - concentration at 60˚C)/60)
H_2	0 .0019	0 .00115	0 .0000125
N_2	0 .029	0 .01	0 .000316667
CH_4	0 .04	0 .012	0 .000466667
CO	0 .045	0 .01	0 .000583333
He	0 .04	0 .0013	0 .000645
O_2	0 .07	0 .0225	0 .000791667
Ar	0 .1	0 .03	0 .001166667
C_2H_6	0 .13	0 .02	0 .001833333
C_2H_4	0 .28	0 .12	0 .002666667
CO_2	3 .45	0 .6	0 .0475
H_2S_2	7	1 .5	0 .091666667
Cl_2	10	3 .2	0 .113333333
SO_2	225	25	3 .333333333
NH_3	900	180	12

Table 5: Solubility indicators for pure gases. **Note:** The solubility indicator was calculated by subtracting a gas's concentration in water arbitrarily chosen at 60 °C, from its equally arbitrarily chosen concentration at 0 °C and dividing it by 60 ((concentration in g gas/ kg water at 0 °C)-(concentration in g gas/ kg water at 60 °C)/60). It is summarized here for gases at one atmosphere under air with a normal composition. Data were found in the Engineering toolbox. This indicates what gases are more soluble than CO_2, and consequently have already escaped the ocean when CO_2 has escaped; such data are not readily available for SF_6.

These ocean emitted gases ascent to the stratosphere at the equator where they are interpreted here to cause ozone depletion [96]. Global stratospheric ozone anomalies were indeed described by Hassler et al. as related to aerosol emissions and they depicted a clear decrease in stratospheric O_3 percentages over time [30]. The figure 6 of Hassler et al. is even reminiscent of the warming stripes of Hawkins [98]. A thinning stratospheric ozone layer gives stratospheric cooling and global tropospheric warming [33].

Pollutants also enhancing seasonal CO_2 uptake: Yearly ocean CO_2 uptake (ML_{YD}) is interpreted here as related to a growing volume of cold arctic water forming each year, because of a larger amount of industrial pollutant emission is expected to results in more heat generated each year and a larger volume of melted ice [99]. Atmospheric CO_2 uptake can be seen as related to the sea-ice melting processes.

Atmospheric increase in CO_2 concentration: The atmospheric increase in CO_2 concentration (G_{ATM}) has been demonstrated in the results above to represent the difference between yearly CO_2 ocean emission and its uptake. It has a R^2 in correlation to UKESM1 that is 9% higher than the average of the sum of emission and uptake. This suggests that some of the atmospheric growth in CO_2 concentration cannot be explained by the UKESM1 pollutant emission alone. First of all, UKESM1 does not cover all the pollutants as Secondary Organic Aerosols having a probable albedo effect are less represented [76]. Some of the atmospheric growth in CO_2 concentration can also be explained by the greenhouse effect of all the gases escaping from

the warming northern Pacific sea surface. In this way they contribute to further emission while they travel up to the stratosphere, as for instance other gases more soluble than CO_2 (Table 5). Finally this difference can also be explained by the pollutants brought directly into the stratosphere during air transport or by being produced at such high temperatures (for instance cement [100]) that the pollutants end up directly in the stratosphere. Each and all of these processes together in various ratios can be seen to contribute to the acceleration of the dominance of the Northern Pacific Ocean CO_2 emission over its uptake.

Duration of CO_2 emission versus CO_2 uptake: Starting 1980, the duration of yearly ocean emission increased (Figure 10). Yulin et al. show that changes in the rate of decrease in sea ice extent occurred by the end of the nineties of the former century [79]. In recording the moment of highest CO_2 uptake each year, the start of the uptake season is seen to shift very mildly from April to May while yearly ocean emission starts earlier in August instead of September (Appendix 13). This results in a slightly shorter uptake period as such intensifying the difference between ocean CO_2 emission and Ocean CO_2 uptake.

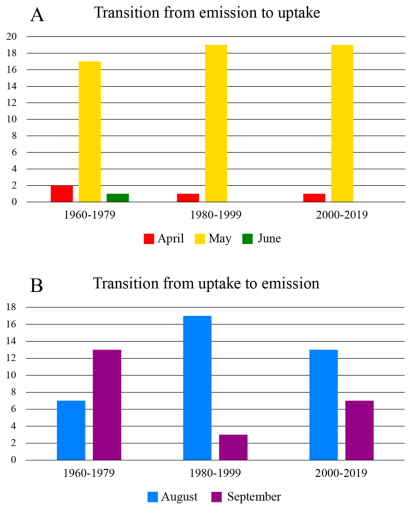

Figure 10: Analysis of how the emission season became longer than the uptake season, for 60 years, each time considering 2 decades. **Note:** A. transition from emission to uptake moves to a later period. B. transition from uptake to emission moves to an earlier period.

The Northern Pacific Carbon Equation

As demonstrated in the results, the Global Carbon Equation (GCE) is neither in balance nor does the statistical analysis of the relation between is components support its present formulation. There is consequently reason to explore a new hypothesis for what determines the Keeling curve in the Northern Pacific Ocean. It can be expressed as follows:

"Pollutants cause tropospheric arctic winter ozone accumulation resulting in a relatively warm self-lofting chemically reactive air bubble (SCHWAB) starting its ascent as soon as light returns to the high latitudes. The trajectory of the SCHWAB influences and is influenced by existing pressure systems and causes storm intensification. The storm intensification results in the incorporation of part of the arctic heat anomaly into the Northern Pacific Ocean. The warmed Northern Pacific Ocean releases its gases because the solubility of gases depends on the temperature of the water they are in. The arctic heat anomaly is probably fully consumed by vaporisation and the oceans do not warm up cumulatively through the intensification of the arctic heat anomaly but through the ocean emitted gases ascending to the stratosphere where they deplete ozone. The stratospheric ozone depletion results in stratospheric cooling and in turn global tropospheric warming and global CO_2 emission."

When expressing this new hypothesis in an equation, the Northern Pacific Carbon Equation (NPCE), the atmospheric increase in CO_2 concentration can be re-defined as:

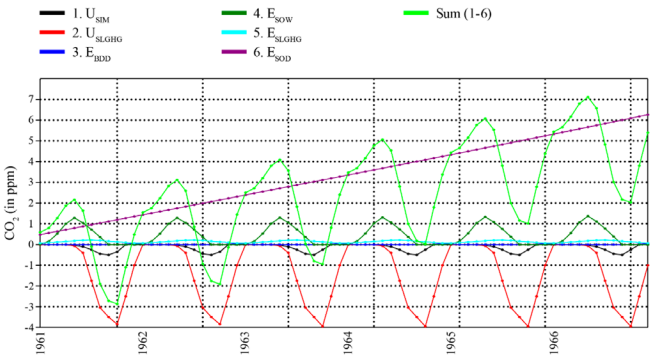

Figure 11: Details of the 6 functions that determine the uptake and emission of CO_2 by the northern Pacific Ocean and their sum (∑1-6). **Note:** (1) Black: ocean CO_2 uptake following from an increase in ocean water solubility due to ocean cooling related to seasonal ice melt (U_{SIM}). (2) Red: increase in ocean CO_2 uptake following from an increase in ocean water solubility due to ocean cooling related to seasonal melt driven by the short lived GHG (U_{SLGHG}). (3) Blue: ocean CO_2 emission through failing biological draw down (E_{BDD}). (4) Dark green: ocean CO_2 emission following from a decrease in ocean water solubility due to seasonal ocean warming (E_{SOW}). (5) Turquoise: increase in ocean CO_2 emission following from a decrease in ocean water solubility due to ocean warming related to seasonal tropospheric heat anomaly stemming from the short lived GHG accumulation in the Arctic (E_{SLGHG}). (6) Purple: CO_2 emission from cumulative ocean heat uptake throughout the year because of ozone depletion in the stratosphere, (E_{SOD}). (7) Apple green: monthly sum of all these functions (Sum 1-6).

$$G_{ATM}=(E_{SOW}+E_{SLGHG}+E_{SOD})-(U_{SIM}+U_{SLGHG}+U_{BDD}) \quad (11)$$

Where:

E_{SOW}: Ocean CO_2 emission following from seasonal ocean warming. This function is stationary as it relates to the inclination of the Earth axis.

E_{SLGHG}: Increase in ocean CO_2 emission caused by the heat generated by the (Short Lived) greenhouse gas in the SCHWAB. This increase in ocean emission is made proportional to pollutant emission. It is stationary as with the evaporation of the latent heat generated by the yearly Arctic heat anomaly is probably fully consumed.

E_{SOD}: Ocean CO_2 emission caused by stratospheric ozone depletion. Stratospheric ozone depletion follows from ocean emitted GHG ascending to the stratosphere because of the warming ocean. This stratospheric ozone depletion gives tropospheric warming and is made proportional to pollutant emission. This function is made cumulative as stratospheric ozone depletion is presently irreversible.

U_{SIM}: Ocean uptake in atmospheric CO_2 following from the seasonal ice melt increasing ocean water solubility (related to the inclination of the Earth axis). This function is stationary as it relates to the inclination of the Earth axis.

U_{SLGHG}: Increase in ocean uptake in atmospheric CO_2 following intensified ocean cooling caused by the short lived GHG in the Arctic heat anomaly. This increase in ocean uptake is made proportional to pollutant emission. It is stationary as the ocean cooling and hence the CO_2 uptake stops as soon as the ice starts accreting again and cold water isn't added to the ocean anymore.

E_{BDD}: Ocean emission in atmospheric CO_2 related to a dysfunctional biological CO_2 drawdown caused by El Niño events off the coast of Peru [80]. The best impression of how these functions intertwine can be obtained when zooming in on a shorter period at the beginning of the relevant period, before the cumulative function drags all other functions apart (Figure 11).

When adding the atmospheric CO_2 concentrations measured at Mauna Loa by the NOAA in May 1961 up (Appendix 10) to the sum of all functions in the following way:

$$G_{ATM}=((E_{SOD}+E_{SLGHG}+E_{SOW}) - (U_{SLGHG}+U_{BDD}+ USM)) + 316{,}89 \text{ ppm} \quad (12)$$

And comparing the data set for each month as offered by the NOAA to the function expressed with the above equation (Figure 11) with a regression analysis generated by the statistical program PAST it is found that they are practically identical. Indeed the probability that the two are not identical is 0 (p=0), and they have a determination coefficient of 0.9989 (Figure 12).

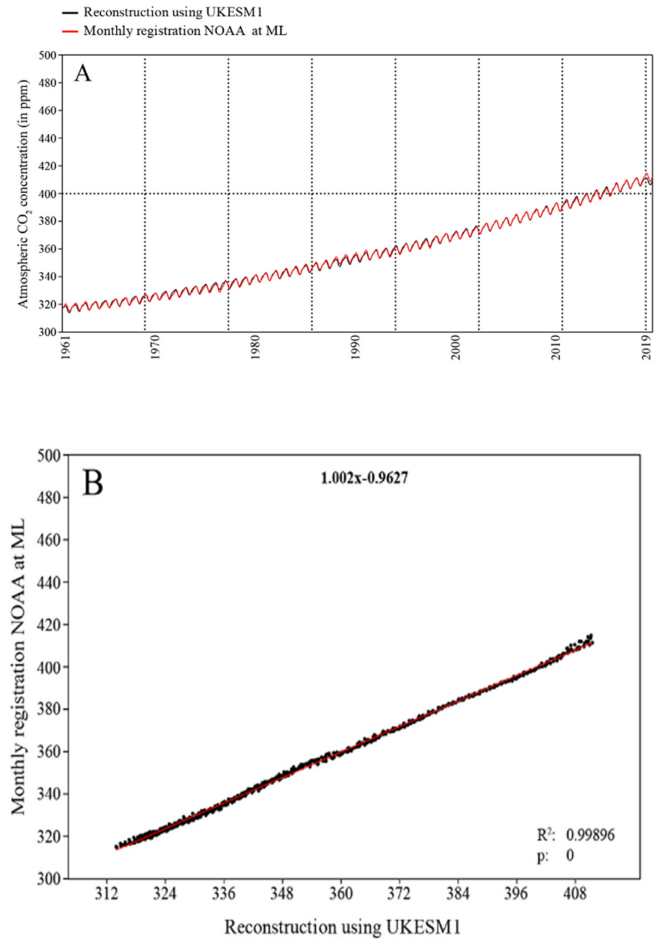

Figure 12: Comparing the monthly reconstruction of the Northern Pacific Carbon Equation (NPCE) basisd on the assumption it is pollutant driven, and the monthly atmospheric CO_2 concentrations recorded by NOAA at Mauna Loa. **Note:** A. Function (black) expressing the reconstructed pollutant driven north Pacific CO_2 emission behaviour ($G_{ATM\ ML\text{-}MONTH}$) compared to (red) the monthly recording of the CO_2 concentration at Mauna Loa as placed online by the NOAA. B. The regression analysis comparing both functions. Details of the functions are given in Appendix 10.

The various components of the Northern Pacific Carbon Equation are presented in detail as macros in Appendix 10 and are explained further in the following.

Stationary symmetrical and asymmetrical functions

Seasonality manifests itself nearly identically in both hemispheres. True seasonal ocean emission through warming (E_{SOW}) and seasonal ocean uptake through seasonal Arctic melting and hence ocean cooling (U_{SIM}), are determined by inclination of the earth's axis and are consequently symmetrical on a yearly basis.

The emission was spread to match day length. Various latitudes for day length were explored but the highest latitude gave the best results, thus indicating the Northern Pacific Ocean is strongly influenced by the Arctic. Industrialisation manifests itself chiefly in the northern hemisphere through the accumulation of pollutants during the arctic polar night when photolysis is impeded.

In the northern hemisphere industrial pollutant emission first causes a mild increase in CO_2 uptake (and other gases, many being more soluble than CO_2, see Table 5) after it causes an intensified ocean gas emission where the SCHWAB appears not only to be self-lofting but also self-enriching in GHG, thus making the industrial influence asymmetrical on a yearly basis.

A cumulative function

The solubility of gases at various temperatures (Table 5) indicates that when CO_2 is emitted, H_2S_2, Cl_2, SO_2 and NH_3 are also emitted. In this respect sulphur dioxide (SO_2) and chlorine (Cl_2) are extremely relevant as their emissions into the stratosphere cause ozone loss when the chlorine (Cl_2) loading of the stratosphere is high [101].

Sulphur hexafluoride (SF_6) also needs mentioning as it is both a very potent GHG and it is reacting with stratospheric ozone [102]. Atmospheric SF_6 has been increasing and the asymmetrical distribution pattern between the northern and the southern hemisphere suggests it reflects the same type of processes as those described here for CO_2 [103].

These temporary chemical ocean warming effects are considered here to cause the global stratospheric ozone depletion that gives stratospheric cooling and in return global tropospheric warming again [33]. This tropospheric warming explains the gradual increase in global ocean CO_2 emission (E_{SOD}) and was made proportional to the UKESM1 function [76].

The biological pump (E_{BDD})

The relation between the ocean sinks (S_{OCEAN}) and the yearly G_{ATM} at Mauna Loa (Figure 13), shows that the two are co-varying [75]. This seems to indicate that as the northern hemisphere gets warmer the ocean CO_2 sinks become larger, which is conceivable as more cold water means more CO_2 uptake.

This chemical effect is feeding both the CO_2 solubility pump and the biological pump because cold water simply contains more dissolved gases which will serve the biological CO_2 drawn down.

The solubility and the biological pump are consequently impossible to disentangle but the biological pump has no bearings for the S_{OCEAN}, and thus the G_{ATM}. Nonetheless, considering the potential weakening of the Atlantic MidOcean Circulation and knowing that the El Niño southern Oscillation is part of the general ocean ventilation, the slowing down of the AMOC was expressed as regular CO_2 emission [104,105].

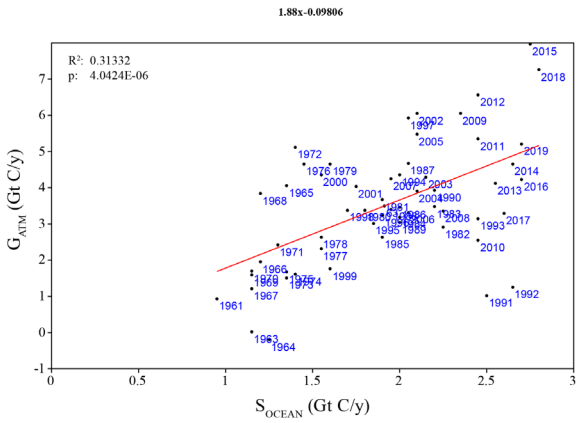

Figure 13: Ocean CO_2 Sinks (S_{OCEAN})and yearly northern Pacific CO_2 (ML_{YD}) uptake compared. **Note:** Regression analysis comparing the 827 ocean sinks (SOCEAN) [75] and yearly atmospheric growth GATM as measured at Mauna Loa. Regression analysis comparing the ocean sinks (S_{OCEAN}) and yearly atmospheric growth G_{ATM} as measured at Mauna Loa.

Fitting the NPCE in the Pleistocene climate cycle

The sawtooth pattern identified by Maslin and Brierly in the four last Pleistocene climate cycles [106, 107]. Indicates that each cycle is typified by slow cooling (approximately 100,000 years) and rapid warming (approximately 10,000 years). These cycles are typically accompanied by a slow increase and a rapid decrease in dust concentration (Figure 14). When introducing the stratospheric ozone cycle into a Pleistocene climate cycle, slow cooling has to reflect slow stratospheric ozone accumulation, while rapid warming has to reflect rapid stratospheric ozone depletion causing earth surface warming. The CO_2 concentration in the ocean being directly linked by the Le Chatelier principle to water temperature, this means that stratospheric ozone accumulation causes oceans to take up more CO_2 than they release, while stratospheric ozone depletion causes oceans to release more CO_2 to the atmosphere. For the Pleistocene the focus is on dust and charcoal (aerosols/ particulates), as both are inversely proportional to CO_2 and temperature [107]. We examine here how the natural organic compounds (VOC'S) and pollutants that vegetation emanates or produces through (partial) combustion can play a part in these shifting ozone balances.

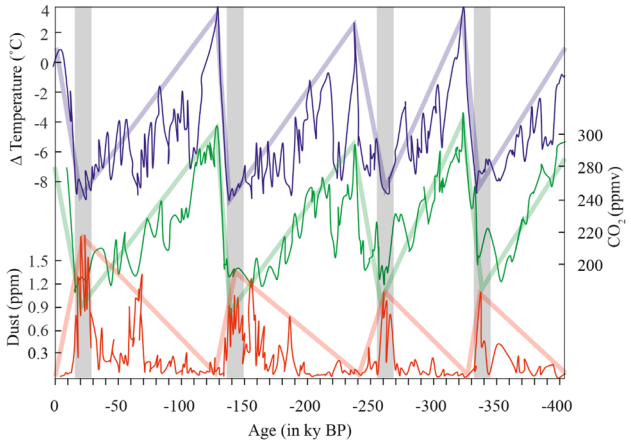

Figure 14: Sawtooth pattern projected on the four last climate cycles. **Note:** Blue lines: temperature anomaly (Δ t in Co), green lines: CO_2 atmospheric concentration (in ppm), red lines: dust concentration(in ppm), grey vertical bar: glacial (after Petit et al. [107]).

Mitigation of the Pleistocene warming phase

Starting at an interglacial maximum and going toward the next glacial maximum, the global kinetic imbalance (OUT>IN) is interpreted as driven by photosynthesis taking H_2O and CO_2 out of the troposphere into vegetation and sinks, but leaving O_2 behind (CO_2+H_2O=> $C_6H_{12}O_6$ (organic molecule)+O_2). This leads to an ever more oxygen rich and inflammable troposphere. In this early cooling phase, the air is warm and damp, forms condensation clouds rather than ice clouds and fire is rare, the cirrus cover is minimal is minimal as the tropopause, which altitude can be seen as thermally defined, has just expanded [108]. Forest fires have approached their minimum due to profuse precipitation and heat favouring angiosperms over gymnosperms. The heat reflected by both the condensation clouds and the earth surface during the early cooling phase can escape rapidly from the troposphere. Because forest fires are scarce, the SCHWAB, generated by these forest fires, is weak and little ocean emitted gases accompanied it to the stratosphere. Water, CO_2 and potentially reactive molecules like VOC, NO and CO [109] are incorporated in the vegetation and its sinks and tropospheric ozone formation is weak, but its stratospheric depletion is even weaker as oceans hardly emit gases. The stratospheric ozone layer is thickening. The stratosphere is warming and the troposphere is cooling.

Mitigation of the Pleistocene cooling phase

Starting at an glacial maximum and going toward the next interglacial maximum, the global kinetic imbalance (IN> OUT) is interpreted as caused by aridity and a high atmospheric O_2 concentration because atmospheric CO_2 and H_2O are buried as organic molecules in sinks. Vegetation that concentrated increasingly in the low latitudes and altitudes is composed chiefly of fire prone gymnosperms occupy a larger proportion of the vegetation cover while angiosperms like Lithocarpus, having relatively high concentrations of inflammable alkanes and a co-evolution with fire peak in the tropics [110]. As the climate cools fire frequency increases due to increasing O_2 concentrations related to the ongoing photosynthesis, but also increases due to the intensification of the aridity related to the colder climate. The self-lofting gymnosperm forest fires inject incompletely combusted organic molecules and other pollutants into the tropopause where they form IPN to the cirrus clouds [111]. The cooling to warming threshold is attained when the SCHWAB fed by the pollutants from the forest fires that reached the Arctic, is large enough to cause the storms that will incorporate the natural arctic heat anomaly into the oceans.

This is when the ocean starts degassing, a.o. CO_2, but much more importantly chlorine (Cl_2), sulphur dioxide (SO_2) or ammoniac (NH_3) being much more soluble and reactive with ozone than CO_2. The spectacular reactivity with ozone of gases like C_2H_2/Ar/O_2, being slightly less soluble in water than CO_2, do need mention in this context. Indeed warming conditions just beyond those allowing for CO_2 emission conditions can result in C_2H_2/Ar/O_2 degassing which deplete stratospheric ozone very rapidly [112]. Such intense and sudden ocean gas emissions cause the stratospheric ozone depletion that introduces the Pleistocene warming phase.

A vegetation/stratospheric-ozone response system

The Pleistocene climate cycle is interpreted here as determined by vegetation composition, which fire frequency influences the quantity of the airborne pollutants. These pollutants determine the size of the SCHWAB, and consequently the degree of the storm intensification. This intensification determines the nature and the quantity of the ocean released gases that react with stratospheric ozone.

Gaia revisited

The pollutant formation in the natural Pleistocene climate cycle reflects a response system between the vegetation composition and the thickness of the ozone layer. Cooling circumstances reduce the expansion of the deciduous angiosperms while favouring the expansion of the conifer forests having a regenerative cycle through fire. When a fire pollutant threshold is crossed the SCHWAB intensifies sufficiently for the Northern Pacific pressure systems to unleash the ocean gases that deplete the stratospheric ozone and the warming phase is initiated. The warming circumstances restore the ratio between angio and gymnosperms, pollutant emission is reduced, the SCHWAB weakens and stratospheric ozone can accrete again.

This interpretation of the Keeling curve echoes the response system of Lovelock [12] between algal blooms and cloudiness, known as the Gaia theory, but here the drivers are pollutants from fires and the response system is between the stratospheric ozone and the vegetation composition.

This model is partly complementary to the model of Ellis and Palmer leaning on the albedo of the polluted ice intensifying Milankovitch eccentricity cycles. But during the Pleistocene the climate cycles become slightly longer each time, do not really match the eccentricity cycles but can be seen as modulating them (Figure 15) [113].

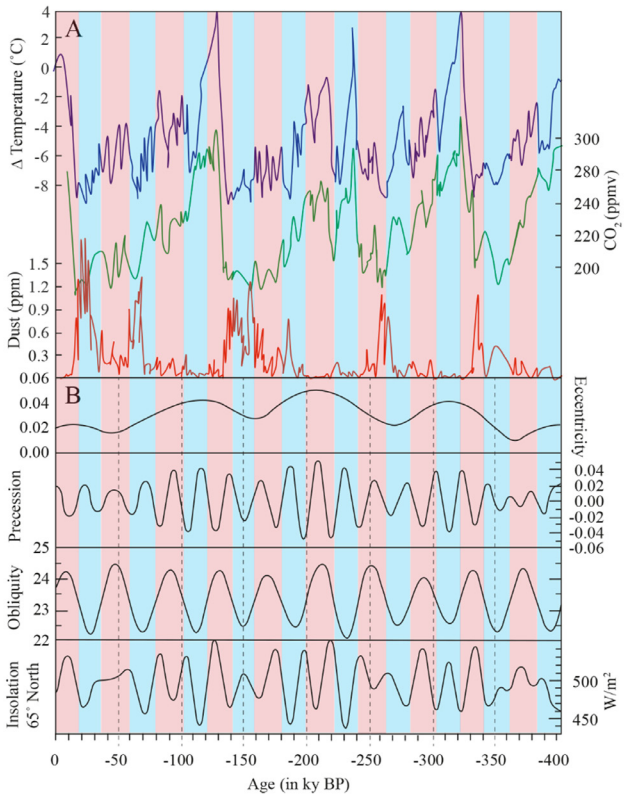

Figure 15: Comparison between the four last climate cycles and the Milankovitch cycles. **Note:** Blue: temperature, Green: CO_2, red: dust. Red shading: high obliquity, blue shading: low obliquity (after Petit et al. [107]). B. Milankovitch cyclicities (after Berger and Yin [121]).

A complex stacked function in the Pleistocene

Also, quite clearly, when comparing the Milankovitch cycles of Berger and Yin to the past four Pleistocene climate cycles obliquity does modulates temperature, as a high obliquity gives warming and a low obliquity gives cooling, whereas precession does the contrary but again these cycles have periods being differing from the vegetation driven ones and are superimposed on the latter [114].

Three sunspot related cycles (unnamed ~9.7-ka; 'Heinrich-Bond' ~6.0-ka; Hallstatt ~2.5-ka), have also been demonstrated to play a minor but periodic role in Earth's climate forcing during the Pleistocene, these reflect functions that are also superimposed on the other ones [115].

The Pleistocene temperature curve, composed of numerous superimposed functions, is strongly serrated and also requires events of higher and more irregular frequencies to explain the observed patterns. Historical evidence of volcanism, being irregular can also be seen to determine the temperature and CO_2 patterns from the Pleistocene. Indeed eruptions are known to have an impact on climate [9]. Insight in volcanic intensity and frequency supports this [116].

Meteorites also can have an impact as they produce high concentrations of dust in the stratosphere as was measured with the Chelyabinsk meteorite [117]. Meteorites strike Earth's atmosphere annually, but bigger impacts occur at century or millennium frequency [118]. Meteorites consequently, can cause unexpected serration to the Pleistocene temperature curve and in its wake, the atmospheric CO_2 concentration.

Finally, grazers may have impacted the length of the cooling period by rapidly promoting the fire prone grasslands over forested areas [119]. This complex co-evolutionary process offers an explanation for the lengthening of the cooling period. Thus grazing known to supress forest growth can be considered to have resulted in the lengthening of the cooling period of each Pleistocene climate cycle.

Industry mimicking the Pleistocene warming phase

What was sketched above is a natural Pleistocene climate cycle, but industrial emissions producing pollutants can have the same effect [14]. Considering the influence that the Brewer Dobson Cell has on stratospheric gas mixing, industrially emitted gases can be seen to impact ozone indirectly through transport to the poles or through direct hot injection in the stratosphere. A relation between ozone depletion and climate is not contested in the IPCC reports, but since 2007, the causality of relation has often been inverted in the scientific literature, in spite of earlier work demonstrating that aerosols cause stratospheric ozone depletion [30,44,120].

Where are we now within the Pleistocene climate cycle?

In the past 140 000 years, there were 110,000 years of cooling and 10,000 years of warming while the interglacial maximum had a duration of approximately 10,000 years, comprising about 5000 years of climatic stasis and 5000 years probably representing a slow start of the cooling phase [121]. The amplitude of the temperature during the Pleistocene was of 10 to 12°C, and the amplitude of the CO_2 concentration was of 100 to 120 ppm. This indicates that (on average!) cooling took place by 0.1 degree Celsius and 1 ppm CO_2 every 1000 years, while warming was of approximately 1°C and 10 ppm /1000 years. Warming in the natural cycle was consequently about ten times faster than its cooling. During the long Pleistocene cooling phase minor uptake imbalance events were only required to occur once every 1000 years. During the short warming phase ocean CO_2 emission required an imbalance every 10 years.

During the past 60 years, ocean emission as measured at Mauna Loa by the NOAA was of approximately 120 ppm of CO_2. As this dramatic excursion of the atmospheric CO_2 has the amplitude of a glacial cycle, and considering that it took place 100 x faster than during a natural warming phase, it cannot be said that it is accidental.

In considering the Pleistocene climate cycles (Figures 14 and 15), it is clear that we are at the top of an interglacial, and in scrutinizing numerous glacial records of oxygen isotope data and pollen records at both high and low latitudes [122] there is good reason to consider that the interglacial maximum has been passed and the cooling cycle was on its way. It is therefore defendable that present aberrantly high atmospheric CO_2 concentrations indicate that anthropogenic industriousness has reiterated the mitigation of cooling conditions from the glacial maximum of the Pleistocene climate cycle.

Two CO_2 air masses at two different altitudes and two different latitudes of the northern hemisphere, indicate that it takes about one year for the SCHWAB to migrate from the Arctic to get to the top of the Hadley cell [80]. Under natural climatic stasis circumstancess, as the interglacial maximum we have reached presently should have been, one would probably not expect the new air mass to already present itself while the old one is still escaping the troposphere.

Discussion

Because the above findings are in various aspects in apparent contrast to the laws of physics, chemistry or biology, it is essential to return the original definitions for the fate of industrially emitted CO_2, the role of light-absorbing particles or GHG, the ocean pH, the role of volcanic material and sea spray, the ozone cycle, the limits of the global carbon pump, and the fragility of our insights on carbon dioxide emission due to land use change.

Where did the industrially emitted CO_2 go?

When explaining the atmospheric increase in CO_2 concentration merely through stratospheric ozone depletion, the question arises why is the industrial CO_2 emission not perceived in the troposphere?

The study of El Niño events responsible for a CO_2 concentration anomaly in the mid troposphere [80] sheds light on this matter. This study indicates that the CO_2 produced at relatively high sea surface temperature rises to 6 km within 4 months. This relatively high sea surface temperature is an "anomaly" of less than 1C° [123]. This indicates that the ascending speed of that CO_2 holding air mass, being initially but 1 degree celcius warmer than the ambiant air, is approximately of 2 m/hour.

At 0.7 m from a domestic chimney employing coal, lowest temperatures are 178 C° [124]. The exhaust temperature of gas vehicles varies between 150 and 600 C° while the analysis of the European waste heat potential has industrial categories that start at 100 C° and end at >1000 C° [125,126]. Industrial and domestic CO_2, are consequently entering the troposphere at "temperature anomalies" of minimally 100 C° and can be expected to rise at 200 m/hour. This indicates that gases entering the troposphere at such temperature cannot be expected to accumulate in the troposphere, but rather to reach into the stratosphere, while the cirrus clouds sieve out the particulates. These considerations support the view that what is measured at Mauna Loa is not industrial CO_2 accumulation, but a flow of gases escaping the warming Northern Pacific Ocean. It must consequently be concluded that the Keeling curve reflects the acceleration of ocean warming, proportional to industrial pollutant emission.

Where are the ocean gases coming from?

The formation of oceanic carbon sinks gives an imbalance in the global carbon budget and is believed to reflect sequestration of the carbon into shelf and ocean sediments. This imbalance can be solved by considering that the mid-ocean ridges have heightened nutrient flows when active [127,128] and constantly feed the oceans with gases. The gases are transferred at each transition from a glacial to an interglacial maximum from the oceans to the atmosphere.

Polyatomic molecules and other light-absorbing aggregates

The words of Lovelock and Margulis: "CO_2 at high concentrations could have performed a similar function as could other polyatomic gases" refer to the fully hypothetical model developed for the early Archean, when it was assumed that the young Sun was faint. By now the faint Sun paradox is found to be questionable [12,129]. A higher rotation velocity of the early Earth could also have caused Earth to be warmer [130]. These are decisions, rather than results, pertaining to a hypothesized deep past. We are now focussing on the past 2.5 million years where the troposphere is chiefly composed of N_2 and O_2, and where H_2O, with an average concentration of 0.4% is the most frequently occurring polyatomic molecule in the atmosphere after which CO_2 follows far behind. Without any doubt all electrons within all atoms of these molecules when excited by light in the outgoing range of the light spectrum and when falling back to a lower energy level will emit more or less infrared light and as such participate in the earth's kinetic budget, but the most frequent more than other compounds. Water vapour is the most frequent and its absorption spectrum clearly encompasses that of other polyatomic molecules in the troposphere. Furthermore pollutants also occur frequently in the troposphere, alkenes, for instance, represent an important fraction of the airborne particulates [131]. Particulate matter, especially has high atmospheric concentrations in the Ganges valley can cause radiative absorption [132]. The hypothetical choice of CO_2 for a debatable problem in the Archean, should be treated with a correct sense of proportionality.

An a-typical ocean pH for the Hawaiian upwelling

Given that the oceans, on a yearly basis, take up less CO_2 than that they are releasing, CO_2 uptake cannot be causing the oceans to decrease in pH, and consequently the cause for this changing pH must be sought for elsewhere. Indeed, the alkalinity changes measured in the ocean appear to be in contradiction with the present ocean degassing model [133].

The temperature dependence of pH and pCO_2 in ocean systems, requires a new interpretation for the covariance between the atmospheric CO_2 recorded at Mauna Loa Observatory and the nearby ocean station ALOHA for which the study of Dore et al. set the tone. Here wet atmospheric air and the pCO_2 in ocean water are inversely proportional on a yearly basis but indeed increase both [134]. This increasing pH is interpreted there as caused by the uptake of atmospheric CO_2, but is assigned in here to the intensification of seasonal storms carrying cold nutrient rich water to the ocean surface and thus stimulating the calcium carbonate production ($CaCO_3$) which drives the ocean water pH down [135]. When considering the pH at in situ temperature, we see it decreases from spring equinox to autumn equinox, thus clearly reflecting a decrease in pH determined by increasing temperature. It consequently is what happens in that period that is relevant to understand the pH and the pCO_2 registered at the ALOHA ocean site. In this context Calil and Richards show that Hawaii is an atypical situation for the whole Northern Pacific as it is influenced by upwelling and that starting September the ocean is cooling, and the pH is thus climbing again [136].

The increasing intensity of such cooling upwelling settings over time has been associated with the recent climate warming conditions [137]. The sea water temperature, the pCO_2 and the pH at the ALOHA ocean site, consequently can be seen to reflect upwelling intensification, while the overall atmospheric CO_2 signal is determined by the Northern Pacific as a whole.

Volcanic particulates and sea spray

When the Krakatau explosion of 1883 caused global cooling, Abbot and Fowle highlighted sulphur as the components of the haze that obstructed solar radiation. By now various volcanic products are considered to be excellent INP [138,139]. There is consequently no reason to associate cooling to sulphur clouds. Volcanoes are all different, depending on their genesis and their position relative to the oceans. Pering et al. for instance, demonstrate that, for the La Fossa crater, Vulcano island, and the North East Crater of Mt. Etna, the sulphur production varied between 4% and 1% of their water production. Volcanoes are also producing ash clouds, the composition of which is primarily siliceous [140,141]. Volcanoes, injecting both water and ash in the atmosphere, are the way, par excellence, to form ice nucleating particles (INP) [142]. In fact successful efforts have even been made at reducing sulphur emission [143]. So, it cannot really be the dimethyl sulphides that will be dimming solar radiation, but rather it is the altitude at which such particulates reside, given their density and origin, that will determine their role in our climate cycle.

The ozone cycle

Despite the 1987 Montreal protocol aiming at the global reduction of the CFCs (chlorofluorocarbons), a global increase in atmospheric concentrations of CFC-11 or hexafluoroethane CF_6 was observed in the last decade [144]. Moreover, there is direct participation of polar stratospheric cirrus in the polar stratospheric ozone depletion *via* sunlight-giving photochemical reactions in spring, for which notably Hydrogen Oxide radicals (HOx), Nitrogen Oxides (NO_x) and sulphur are responsible [145]. This is in strong support of satellite-observed warming pattern that resembles the atmospheric distribution of Chlorofluorocarbons (CFCs) [146].

Asymmetric ozone distribution patterns comparable to those for CO_2 or CH_4 in the troposphere can be witnessed in Bednarz et al. [147].

Lightning frequency has increased drastically in the Arctic over the past decade [148]. This increase follows from higher aerosol concentrations in the atmosphere [149]. The predominant mechanism of ozone formation in the upper troposphere is lightning-induced precursors such as oxides or pollutants like nitrogen (NO_x), Carbon Monoxide (CO), and Hydrocarbons (HC).

The intensification of industrial and agricultural dust and pollutants like for instance the volatile organic carbons, or isoprene produced by the palm oil industry can be expected to intensify the formation of the SCHWAB over time and hence, the stratospheric ozone depletion [150].

The limits of the biological carbon pump

The boosting of algal blooms is still considered as a means for the restoration of the natural carbon cycle by drawing CO_2 down from the atmo- to the hydrosphere but seeding was unsuccessful [151,152]. The Banda Sea upwelling area explains this as these upwelling waters are feeding each consecutive trophic level with a specific speed and duration adapted to the life cycle of the involved species [153]. Any imbalance in these equilibria developed over time will have a so-called harmonica effect where Fe stimulated algal overproduction results in excessive zooplankton production depleting the area of its oxygen. Parts of the phytoplankton does reach the ocean bottom as faecal pellets holding both inorganic $CaCO_3$ and organic carbon, but the eutrophication through seeding can even cause the toxic Harmful Algal Blooms (HAB) associated with ocean CO_2 emission [154-155].

Albedo or chemically driven global warming

In 2023, direct negative forcing through (aviation) aerosols raised alarm [48]. This suggested that the air transport industry could mitigate global warming in a similar way as Marine Cloud Brightening (MCB) would do. In its latest report the IPCC supported this view that particulates induced albedo could mask the effect of GHG and prepared to lean towards geoengineering, but, in contrast with studies from the 1970, they only focussed on clouds albedo and neglected the possibility that the arctic heat anomaly is induced chemically. From present study it becomes clear that the chemical heat clearly surpasses negative forcing.

Land use change emission, land use change surface

The relation between G_{ATM} and land use change was established above in the results through the new hypothesis that land use change surface (S_{LUC}) increase is responsible for an increase in the production of aerosols and pollutants. Here we see (Figure 16) that land sinks (S_{LAND}) increase with increasing land use change surface (S_{LUC}). E_{LUC} instead of emitting CO_2 to the troposphere, is found here to form a sink, which can be explained as transport to the hydrosphere through consumption and thus disappearing from the troposphere. The extreme eutrophication of the North Sea testifies to this [156].

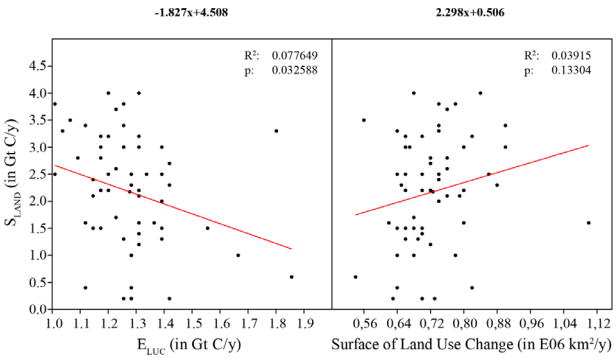

Figure 16: Trend analyses between land sinks (S_{LAND}) and land use change CO_2 emission (E_{LUC}) or surface of land use change (S_{LUC}).

The difficulties at separating between land CO_2 sinks (S_{LAND}) and land use change CO_2 emission (E_{LUC}) was reported by their developers [70]. The evaluation of these two parameters is more complex than commonly believed. Indeed, Hakkarainen et al. show that the tropical rainforests belts are emitting CO_2 [81]. In the most recent publications of June 2024 of a the European Centre for Medium-Range Weather Forecasts we clearly see that, on land, there is CO_2 emission in the southern hemisphere. This is also true when looking at the areas where the Brazil tropical forest did not undergo burning and cutting and this holds also for Africa [157-159]. The response of tropical trees to rising temperatures is a key uncertainty limiting our ability to predict CO_2 biosphere-to-atmosphere feedbacks in a warming world. Indeed tropical trees show that the ratio between photosynthesis and respiration intensity is affected by high temperatures for some taxa more than for others [160]. These considerations can explain the paradoxical correlations observed in our statistical analysis of the relation between carbon sinks and sources on land.

Alternatively, the CO_2 emission of tropical forests can also be explained by fungi in soils because fungal respiration rates also increase at increasing temperatures [161]. These paradoxical considerations are mentioned here to urge a reassessment of the impact of agriculture on CO_2 but even more so on organic aerosols.

Stratospheric ozone depletion reflected in emission only

In the present reconstruction of Keeling curve (Appendix 10) the influence of stratospheric ozone depletion was only made to influence

ocean CO_2 emission (E_{SOD}) but not the increase in uptake through the solubility pump. It is therefore highlighted here that present study reflects the northern hemisphere until 2019 where the Arctic was hardly affected by stratospheric ozone depletion, in contrast to the Northern Pacific Ocean at Mauna Loa [162]. Indeed, recent results indicate that stratospheric ozone depletion is prominent in the low and absent in the high latitudes [163].

Angiosperms taking the floor

Since their diversification in the Cretaceous, the angiosperms have outcompeted the gymnosperms that retrieved to colder areas. This overtaking is accompanied with cooling [164]. The cooling from the Mesozoic to the Cenozoic is typically associated with a decrease in atmospheric CO_2 concentrations, accompanied by an increase in amplitude and possibly periodicity [165]. It is suggested here that our Pleistocene vegetation driven climate cyclicity represent the end member of co-evolution between vegetation composition and hydro-, troposphere and stratospheric chemistry and started in the Mesozoic.

Limitations of this study

In spite of the use of numerous approximations, present reconstruction reproduces the monthly Keeling curve well. It demonstrates that the Keeling curve is a symptom of a temperature driven System Earth, in which temperature is determined by a cocktail of industrial pollutants.

The pollutant values taken from Griffiths et al. have a very low resolution [76]. Which required that the monthly values were constructed between two consecutive years (Appendix 10). In spite of Griffiths et al. looking far into the future, predictions aren't developed in the present study, as pollutant production depends on a UN Montreal Protocol type of regulations whose feasibility belongs to the political domain which is far beyond the scope of this paper [76].

Also the bulk chemical transformation taking place in the arctic winter night was touched upon, but requires further investigation, especially in the light of complex four dimensional dynamic processes having varying intensities or accelerations over time. Here, only a modest dysfunction of the La Niña was considered, but upwelling areas are numerous and this function of the NPCE may well have been underestimated.

With respect to the stratospheric ozone depletion, industrial pollutants or excessive ocean emitted gases caught by the higher Brewer Dobson Cell can be expected to contribute to the thickness of the stratospheric ozone layer when, in the downwards flow they come to react with the lower stratosphere.

Also, it appears that radicals are much more diverse than conceived in the context of climate change and require a reassessment, as industrially emitted pollutants and as natural occurrences in ocean systems through fluvial transport like for instance the highly reactive SF_6. In addition, long before we suspect other nations to neglect a UN agreement, one should keep in mind that fluorine compounds, or simple radicals are ubiquitously present in nature, and that further study is required.

So while this study is supported by good statistical results, there is room for intensified biologically driven ocean CO_2 emission, and a potential Brewer Dobson cell "rain" of particulates would require an extra function having a mild influence on some of the other functions. The main contribution that this study represent, is that it offers a new multidisciplinary solution to an earlier GHG driven hypothesis that is inconsistent with the Le Chatelier principle while bringing our knowledge on the stratosphere, troposphere, hydrosphere and biosphere together into one model for both the present and the past.

Conclusion

Our introduction aimed at being exhaustive with respect to all the hypotheses brought to the scientific arena until now and makes it plausible that a pollutant driven had not fully been explored yet.

The atmospheric increase in CO_2 concentration (G_{ATM}), hypothesized to reflect the tropospheric accumulation of industrial CO_2 that was not taken up by our planet's carbon sinks is demonstrated here to reflect the difference between the Northern Pacific Ocean CO_2 emission and its uptake. The Global Carbon Equation is shown to be out of balance by 0.395 Gt C which imbalance reflects the difference between Northern Pacific Ocean seasonal emission and uptake, as interpreted by the WCRP. This imbalance reflects chiefly our difficulties in estimating the CO_2 land sinks and land sources. These difficulties are fundamental in nature and urge new studies.

Because the G_{ATM} as recorded in the Keeling curve is fully explained by the Northern Pacific emission and uptake in CO_2, industrial CO_2 emission is not playing a part. This absence is explained by industrial heat causing CO_2 to self-loft out of the troposphere. In the absence of CO_2 as the GHG causing global warming, pollutants are considered, because they are emanated from crops and G_{ATM} co varies with the surface of land use change, but not the emission of land use change. Such pollutants are hypothesized to be sieved out of the self-lofting industrial emission by forming ice clouds in the tropopause where they are transported to the Arctic. In the arctic winter night, these chemically diverse particulates often transform into the short lived GHG ozone, which in the absence of light allowing for photolysis, accumulates. This ozone rich chemically reactive mixture becomes self-lofting as soon as it gets illuminated in early spring.

The Keeling curve is hypothesized here to reflect the intensification of the existing Northern Pacific pressure systems and the yearly ascent of the self-lofting chemically reactive Arctic winter generated air bubble (SCHWAB) at the low latitudes, but also its ozone depleting consequences in the stratosphere.

This hypothesis was tested by modelling, under the following assumptions: (1) CO_2 uptake depends on seasonal ice melting, (2) CO_2 uptake also results from enhanced melting through pollutant accumulation in the Arctic winter night, (3) seasonal CO_2 emission is related to the health of La Niña (biological pump), (4) seasonal ocean CO_2 emission depends on seasonal warming, (5) the CO_2 emission is also influenced by the incorporation of arctic heat anomaly into the Northern Pacific, and (6) CO_2 emission is caused by the buffering of the ocean emitted gases by the ozone in the stratosphere, resulting in global stratospheric cooling and global tropospheric warming. The sum result of these six functions was found to reproduce the Keeling curve.

The present societal focus on CO_2 emission is an attempt to deal with a symptom while aerosols are being presented lately as causing cooling and thus masking the true GHG warming. It is demonstrated here that the chemical warming effect of these aerosols widely surpasses their effect as cloud brightening seeds.

Present new hypothesis is corroborated by a fire dust-driven Pleistocene response system between vegetation composition and the stratospheric ozone layer, thus reminiscent of the Gaia hypothesis of Lovelock. The cooling phase of the Pleistocene climate cycle, going from the interglacial to the glacial maximum, is mitigated by the increasing frequency of (gymnospermous) forest fires producing natural pollutants that induces the formation of a natural SCHWAB unleashing a broad spectrum of ocean emitted gases depleting the ozone that accumulated in the lower stratosphere during the Pleistocene cooling phase. This results in stratospheric cooling and tropospheric warming. The warming phase, from the glacial to the interglacial maximum, is mitigated by the return to warm, humid and

high atmospheric CO_2 circumstancess reducing the fire frequency by restoring the dominance of the vegetations rich in deciduous (chiefly angiosperm) trees over the vegetations having a fire regenerating cycle (chiefly gymnosperms). This shift in vegetation type ratios allows for the SCHWAB to ascend to the stratosphere without unleashing a broad spectrum of ocean emitted gases, thus giving in ozone accumulation. This results in stratospheric warming and tropospheric cooling.

The present study can be seen to build onto the introductory sentence of the first (1990) IPCC report [34] in the following way:

"We are certain of the following: there is a natural greenhouse effect which already keeps the Earth warmer than it would otherwise be; pollutant, volatile organic carbons in particular, (organic) dust, black carbon and particulate matter emissions resulting from human activities are substantially causing a yearly arctic heat anomaly increasing the atmospheric concentrations of the greenhouse gases: carbon dioxide, methane, chlorofluorocarbons (CFCs), nitrous oxide, and others gases. These increases deplete ozone in the lower stratosphere resulting on average in an additional warming of the Earth's surface."

Acknowledgements

I am grateful for the critical proofreading by Prof. Dr. Ing. JW Erisman, Chair of the Netherlands Scientific Climate Council. I thank Dr S. Kaptein for the fruitful discussion. I am grateful for the editing and proof reading of Prof. dr. T. Van Loon and Dr. WJE van de Graaff. Finally I thank Drs SP Maas for controling the english. and Drs. H Caspers and Mr. EJ Bosch for their help with the illustrations.

References

1. Herschel W (1801) Observations tending to investigate the nature of the sun, in order to find the causes or symptoms of its variable emission of light and heat with remarks on the use that may possibly be drawn from solar observations. Phil Trans Royal Soci London 31(91):265-318.
2. Foote E (1856) Circumstancess affecting the heat of the sun's rays. Am J Sci Arts 22(66):382.
3. Tyndall JI (1861) On the absorption and radiation of heat by gases and vapours, and on the physical connexion of radiation, absorption, and conduction. Phil Trans Royal Soci London. 151:1-36.
4. Held IM, Soden BJ (2000) Water vapor feedback and global warming. Ann Rev Energ Environ 25(1):441-475.
5. Arrhenius S (1896) On the influence of carbonic acid in the air upon the temperature of the ground. London Edinburgh Philos Mag J Sci Apr 41(251):237-276.
6. De Marchi L (1895) The causes of the ice age. Nature 52: 412.
7. Russell FA (1888) Spread of The Phenomena Round the World, with Maps Illustrative Thereof. Erupt Krakatoa Subseq Phenom. 334-9.
8. Archibald D (1888) Diurnal and Secular Variation in the Duration and Brilliancy of the Twilight Glows of 1883-1884 and the Height Above Earth of the Stratum that Caused them. Erupt Krakatoa Subseq Phenom 340-381.
9. Abbot CG, Fowle FE (1913) Volcanoes and climate. Smithsonian Miscell Collect 60 (29): 1-24.
10. Croll J (1864) On the physical cause of the change of climate during geological epochs. London Edinburgh Philos Mag J Sci 28(187):121-37.
11. Sagan C, Mullen G (1972) Earth and Mars: Evolution of atmospheres and surface temperatures. Science 177(4043):52-6.
12. Lovelock JE, Margulis L (1974) Atmospheric homeostasis by and for the biosphere: The Gaia hypothesis. Tellus 26: 1-2.
13. Valley SL (1965) Handbook of Geophysics.
14. Carter LJ (1970) The Global Environment: M.I.T. Study Looks for Danger Signs. Science 169 (3946): 660-662.
15. Mohnen VA, Hidy GH (2011) Atmospheric nanoparticles early metrology and observations (1875–1980). History and Reviews RTI press 411-457.
16. Liss PS (1985) Changing climate: Report of the carbon dioxide assessment committee. National Research Council.
17. Council NR (1979) Carbon dioxide and climate: A scientific assessment. The National Academies Press, Washington DC 10:12181.
18. Liu SC, Kley D, McFarland M, Mahlman JD, Levy H (1980) On the origin of tropospheric ozone. J Geophys Res: Oceans 85(C12):7546-52.
19. Wada Y, Van BLP, Van KCM, Reckman JW, Vasak S (2010) Global depletion of groundwater resources. Geophy Res Let 37(20).
20. Chen X, Jeong SJ (2018) Irrigation enhances local warming with greater nocturnal warming effects than daytime cooling effects. Env Res Lett 13(2):024005.
21. Lovelock JE, Maggs RJ, Rasmussen RA (1972) Atmospheric dimethyl sulphide and the natural sulphur cycle. Nature 237(5356):452-3.
22. Ayers GP, Cainey JM (2007) The CLAW hypothesis: A review of the major developments. Environ Chem 4(6):366-74.
23. Zheng G, Kuang C, Uin J, Watson T, Wang J (2020) Large contribution of organics to condensational growth and formation of Cloud Condensation Nuclei (CCN) in the remote marine boundary layer. Atmosph Chem Physics 20(21):12515-25.
24. Crutzen PJ (1970) The influence of nitrogen oxides on the atmospheric ozone content. QJ R Meteor Soc 96:320-325.
25. Molina MJ, Rowland FS (1974) Stratospheric sink for chlorofluoromethanes: Chlorine atom-catalysed destruction of ozone. Nature 249(5460):810-2.
26. Nielsen OJ, Bilde M (2021) Reflection on two Ambio papers by PJ Crutzen on ozone in the upper atmosphere. Ambio 50(1):40-3.
27. Guez L, Bruston P, Raulin F, Régnaut C (1997) Importance of phase changes in Titan's lower atmosphere. Tools for the study of nucleation. Planetary Space Sci 45(6):611-25.
28. Strawa A, Pueschel R, Ferry G (1998) The roles of aerosols in stratospheric ozone chemistry. Earth Sci Enterpr Atmos Phys 171.
29. Siegmund P, Sigmond M, Kelder H (2004) The stratosphere as a puppeteer of European winter climate. europhysics news 35(3):73-5.
30. Hassler B, Bodeker GE, Dameris M (2008) A new global databasis of trace gases and aerosols from multiple sources of high vertical resolution measurements. Atmosph Chemi Phy 8(17):5403-21.
31. Randel WJ, Polvani L, Wu F, Kinnison DE, Zou CZ (2017) Troposphere-stratosphere temperature trends derived from satellite data compared with ensemble simulations from WACCM. J Geophy Res Atmospheres 122(18):9651-9667.
32. Liu W, Hegglin MI, Checa GR, Li S, Gillett NP (2022) Stratospheric ozone depletion and tropospheric ozone increases drive Southern Ocean interior warming. Nature Clim Change 12(4):365-372.
33. Lin J, Emanuel K (2024) Why the lower stratosphere cools when the troposphere warms. Pro Nat Acad Sci 121(11):e2319228121.
34. IPCC (1992) First Assessment Report Overview and Policymaker IPCC Supplement. Published with the support of Australia, Canada, Germany, The Netherlands, Spain, United States of America, Austria, France, Japan, Norway and United Kingdom.
35. Turco RP, Toon OB, Ackerman TP, Pollack JB, Sagan C (1983) Nuclear winter: Global consequences of multiple nuclear explosions. Science 222(4630):1283-1292.
36. Houghton RA (2007) Balancing the global carbon budget. Annu Rev Earth Planet Sci 35(1):313-347.
37. McNeil BI, Matear RJ, Key RM, Bullister JL, Sarmiento JL (2003) Anthropogenic CO_2 uptake by the ocean basisd on the global chlorofluorocarbon data set. Science 299(5604):235-239.
38. Le Quere C, Raupach M, Canadell J, Marland G, Bopp L, et al. Emissions of organic compounds from western US wildfires and their near-fire transformations. Atmosph Chem. and Phys 22:9877-9893.
39. Ciais P, Sabine C, Bala G, Bopp L, Brovkin V, et al (2014) Carbon and Other Biogeochemical Cycles. Assessment Report of the Intergovernmental Panel on Climate Change Change. Cambridge

University Press 465-570.

40. Friedlingstein P, O'sullivan M, Jones MW, Andrew RM, Bakker DC (2023) Global carbon budget 2023. Earth Syst Sci Data 15(12):5301-5369.
41. Denisov ET (2008) Mechanisms of the reactions of radicals with ozone. Russian J Phys Chem B 2:58-66.
42. Harrison RM (2013) Chemistry of the troposphere. Royal Society of Chemistry 182-203.
43. Pörtner HO, Roberts DC, Poloczanska ES, Mintenbeck K, Tignor M (2022) IPCC: Summary for policymakers.
44. Noel S, Weigel K, Bramstedt K, Rozanov A, Weber M, et al (2018) Water vapour and methane coupling in the stratosphere observed using SCIAMACHY solar occultation measurements. Atmos Chem Phy 18(7):4463-76.
45. Zhao F, Tang C, Dai C, Wu X, Wei H (2020) The global distribution of cirrus clouds reflectance basisd on MODIS level-3 data. Atmosphere 11(2):219.
46. IPCC (1997) Technical Report. Published with the support of Australia, Canada, Germany, The Netherlands, Spain, United States of America, Austria, France, Japan, Norway and United Kingdom.
47. IPCC (2023) Climate Change 2023: Synthesis Report. Contribution of Working Groups I, II and III to the Sixth Assessment Report of the Intergovernmental Panel on Climate Change.
48. Quaas J, Jia H, Smith C, Albright AL, Aas W (2022) Robust evidence for reversal of the trend in aerosol effective climate forcing. Atmos Chem Phy 22(18):12221-39.
49. Kok JF, Storelvmo T, Karydis VA, Adebiyi AA, Mahowald NM (2023) Mineral dust aerosol impacts on global climate and climate change. Nature Rev Earth Environ 4(2):71-86.
50. Julsrud IR, Storelvmo T, Schulz M, Moseid KO, Wild M (2022) Disentangling aerosol and cloud effects on dimming and brightening in observations and CMIP6. J Geophy Res Atmos 127(21):e2021JD035476.
51. Zhao N, Dong X, Huang K, Fu JS, Lund MT (2021) Responses of Arctic black carbon and surface temperature to multi-region emission reductions: A Hemispheric Transport of Air Pollution Phase 2 (HTAP2) ensemble modeling study. Atmos Chem Phy 21(11):8637-54.
52. Liss PS, Lovelock JE (2007) Climate change: The effect of DMS emissions. Environ Chem 4(6):377-8.
53. Friedel M, Chiodo G (2022) Ozone depletion over the Arctic affects spring climate in the Northern Hemisphere. Nature Geosci 15(7):518-9.
54. Chartrand DJ, De Grandpré J, McConnell JC (1999) An introduction to stratospheric chemistry: Survey article. Atmosphere Ocean 37(4):309-67.
55. Law KS, Hjorth JL, Pernov JB, Whaley CH, Skov H (2023) Arctic tropospheric ozone trends. Geophy Res Lett 50(22): e2023GL103096.
56. Baker AR, Laskina O, Grassian VH (2014) Processing and ageing in the atmosphere. Mineral dust 2014:75-92.
57. Van DKS, Wang X, Kershaw P, Guichard F, Setiabudi DA (2000) A Late Quaternary palaeoecological record from the Banda Sea, Indonesia: patterns of vegetation, climate and biomass burning in Indonesia and northern Australia. Palaeogeo Palaeoclimatol Palaeoecol 155(1-2):135-53.
58. Han Y, An Z, Marlon JR, Bradley RS, Zhan C (2020) Asian inland wildfires driven by glacial interglacial climate change. Proc National Academy of Sciences 117(10):5184-9.
59. Rickly PS, Guo H, Campuzano JP, Jimenez JL, Wolfe GM (2022) Emission factors and evolution of SO_2 measured from biomass burning in wildfires and agricultural fires. Atmosph Chem Phy 22(23):15603-20.
60. Fernandes DE, Salgueiro V, Costa MJ, Lucio PS, Potes M (2023) Fire-Pollutant-Atmosphere Components and Its Impact on Mortality in Portugal During Wildfire Seasons. Geohealth 7(10):e2023GH000802.
61. Senf F, Heinold B, Kubin A, Müller J, Schrödner R (2023) How the extreme 2019-2020 Australian wildfires affected global circulation and adjustments. Atmos Chem Phy 23(15):8939-58.
62. Nguyen DH, Lin C, Vu CT, Cheruiyot NK, Nguyen MK (2022) Tropospheric ozone and NO_x: A review of worldwide variation and meteorological influences. Envn Technol Inn 28:102809.
63. Mansergas A, Anglada JM (2007) The gas-phase hydrogen-bonded complex between ozone and hydroperoxyl radical. A theoretical study. J Phy Chem A 111(5):976-81.
64. Witze A (2020) Rare ozone hole opens over Arctic and it's big. Nature 580(7801):18-20.
65. Barnes EA, Screen JA (2015) The impact of Arctic warming on the midlatitude jet-stream: Can it? Has it? Will it?. Wiley Interdiscip Rev Clim 6(3):277-86.
66. Beilman DW, Massa C, Nichols JE, Elison TO, Kallstrom R (2019) Dynamic Holocene vegetation and North Pacific hydroclimate recorded in a mountain peatland, Moloka 'i, Hawai 'i. Frontiers Earth Sci 7:188.
67. Chen S, Yu B, Chen W, Wu R (2018) A Review of atmosphere–ocean forcings outside the Tropical Pacific on the El Niño-Southern Oscillation occurrence. Atmosphere 9(11):439.
68. Chylek P, Folland C, Klett JD, Wang M, Hengartner N (2022) Annual mean Arctic amplification 1970–2020: Observed and simulated by CMIP6 climate models. Geophy Res Letters 022GL099371.
69. Ballantyne AP, Andres R, Houghton R, Stocker BD, Wanninkhof R (2015) Audit of the global carbon budget: estimate errors and their impact on uptake uncertainty. Biogeosciences 12(8):2565-84.
70. Gasser T, Crepin L, Quilcaille Y, Houghton RA, Ciais P (2020) Historical CO_2 emissions from land use and land cover change and their uncertainty. Biogeosciences 17(15):4075-101.
71. Carbon brief.
72. Hammer Ø, Harper DA (2001) Past: paleontological statistics software package for educaton and data anlysis. Palaeontol Electronica 4(1):1.
73. Tans P, Keeling CD. NOAA
74. Winkler K, Fuchs R, Rounsevell M, Herold M (2021) Global land use changes are four times greater than previously estimated. Nature comm 12(1):2501.
75. Bennington V, Gloege L, McKinley GA (2020) Variability in the Global Ocean Carbon Sink From 1959 to 2020 by Correcting Models with Observations. Geophys Res Lett 9:e2022GL098632.
76. Griffiths PT, Murray LT, Zeng G, Shin YM, Abraham NL (2021) Tropospheric ozone in CMIP6 simulations. Atmos Chem Phys 21(5):4187-218.
77. Hakkarainen J, Ialongo I, Maksyutov S, Crisp D (2019) Analysis of four years of global XCO_2 anomalies as seen by orbiting carbon observatory-2. Remote Sensing 11(7):850.
78. NOAA/GML: Trends in Atmospheric Carbon Dioxide, NOAA Global Monitoring Laboratory. 2024.
79. Yulin AV, Lis N, Egorova E (2019) Interannual and seasonal variability of Arctic sea ice extent according to satellite observations. Russian Arctic 7: 26-35.
80. Peter R, Kuttippurath J, Chakraborty K, Sunanda N. A high concentration CO_2 pool over the Indo-Pacific Warm Pool. Scientific Reports 13(1):4314.
81. Hakkarainen J, Ialongo I, Maksyutov S, Crisp D (2019) Analysis of four years of global XCO_2 anomalies as seen by orbiting carbon observatory-2. Remote Sensing 11(7):850.
82. Thomsen VB (2000) LeChâtelier's principle in the sciences. J Chem Educa 77(2):173.
83. Verma S, Yadava PK, Lal DM, Mall RK, Kumar H (2021) Role of lightning NO_x in ozone formation: A review. Pure App Geophy 178:1425-43.
84. Cox RA, Ammann M, Crowley JN, Herrmann H, Jenkin ME (2020) Evaluated kinetic and photochemical data for atmospheric chemistry: Volume VII–Criegee intermediates. Atmos Chem Phy 20(21):13497-519.
85. Jia H, Li S, Wu L, Li S, Sharma VK (2020) Cytotoxic free radicals on airborne soot particles generated by burning wood or low-maturity coals. Environ Sci Technol 54(9):5608-18.
86. Yu P, Toon OB, Bardeen CG, Zhu Y, Rosenlof KH (2019) Black carbon

lofts wildfire smoke high into the stratosphere to form a persistent plume. Science 365(6453):587-90.

87. Haarig M, Ansmann A, Baars H, Jimenez C, Veselovskii I (2018) Depolarization and lidar ratios at 355, 532, and 1064 nm and microphysical properties of aged tropospheric and stratospheric Canadian wildfire smoke. Atmos Chem Phy 18(16):11847-61.

88. Ditas J, Ma N, Zhang, Y, Assmann D, Neumaier M, et al (2018) Strong impact of wildfires on the abundance and aging of black carbon in the lowermost stratosphere. PNAS 115. 201806868.

89. Peterson DA, Fromm MD, McRae RH, Campbell JR, Hyer EJ, et al (2021) Australia's Black Summer pyrocumulonimbus super outbreak reveals potential for increasingly extreme stratospheric smoke events. NPJ Climate Atmos Science 4(1):38.

90. Bush RT, McInerney FA (2013) Leaf wax n-alkane distributions in and across modern plants: Implications for paleoecology and chemotaxonomy. Org Geochem 79: 65-73.

91. Balzade Z, Sharif F, Anbaran SR (2021) Extending alkenes' value chain to functionalized polyolefins. Intech Open.

92. Schumann U, Bugliaro L, Dörnbrack A, Baumann R, Voigt C (2021) Aviation contrail cirrus and radiative forcing over Europe during 6 months of COVID-19. Geoph Res Let 48: e2021GL092771.

93. Zhu J, Penner JE (2020) Indirect effects of secondary organic aerosol on cirrus clouds. J Gesophys Res Atmos 125: e2019JD032233.

94. Giamalaki K, Beaulieu C, Henson SA, Martin AP, Kassem H, et al (2021) Future intensification of extreme Aleutian low events and their climate impacts. Scientific reports 11(1):18395.

95. Farrar JT, Weller RA (2006) Intraseasonal variability near 10°N in the eastern tropical Pacific Ocean. J Geophys Res 111: C05015.

96. Bisht JSH, Machida T, Chandra N, Tsuboi K, Patra PK, et al (2021) Seasonal variations of SF6, CO_2, CH_4, and N_2O in the UT/LS region due to emissions, transport, and chemistry. J Geoph Res Atmos 126: e2020JD033541.

97. Engineering toolbox.

98. Hawkins E. Warming stripes.

99. Ouyang Z, Qi D, Chen L, Takahashi T, Zhong W, et al (2020) Sea-ice loss amplifies summertime decadal CO_2 increase in the western Arctic Ocean. Nat Clim Chang 10: 678–684.

100. Alobaydy O (2024) Impacts of Cement Production on the Environment with Practical Solutions: A critical review. J Res Technol Eng 5(2): 12-275.

101. Ming A, Winton VH, Keeble J, Abraham NL, Dalvi MC, et al (2020) Stratospheric ozone changes from explosive tropical volcanoes: Modeling and ice core constraints. J Geophy Res: Atmos. 125(11): e2019JD032290.

102. Ni J, Liu S, Lang X, He Z, Yang G (2023) Sulphur hexafluoride in the marine atmosphere and surface seawater of the Western Pacific and Eastern Indian Ocean. Env Poll. 335; 122266.

103. Simmonds PG, Rigby M, Manning AJ, Park S, Stanley KM, et al (2020) The increasing atmospheric burden of the greenhouse gas sulphur hexafluoride (SF6). Atmos Chem Phys 20: 7271–7290.

104. Caesar L, Rahmstorf S, Robinson A, Feulner G, Saba V (2018) Observed fingerprint of a weakening Atlantic Ocean overturning circulation. Nature 556(7700):191-6.

105. Liu W, Duarte C, Pinto D, Fedorov A, Zhu J (2023) The impacts of a weakened Atlantic meridional overturning circulation on ENSO in a warmer climate. Geophy Res Let 50(8):e2023GL103025.

106. Maslin MA, Brierley CM (2015) The role of orbital forcing in the Early Middle Pleistocene Transition. Quaternary International. 389:47-55.

107. Petit JR, Jouzel J, Raynaud D, Barkov NI, Barnola JM,et al (1999) Climate and atmospheric history of the past 420,000 years from the Vostok ice core, Antarctica. Nature 399(6735):429-36.

108. Santer BD, Sausen R, Wigley TM, Boyle JS, AchutaRao K (2003) Behavior of tropopause height and atmospheric temperature in models, reanalyses, and observations: Decadal changes. J Geophy Res: Atmosph. 108(D1):ACL-1.

109. Liang Y, Stamatis C, Fortner EC, Wernis RA, Van Rooy P, et al (2022) Emissions of Organic Compounds from Western US Wildfires and Their Near Fire Transformations. Atmos Chem Phy 2022:1-32.

110. Xiao X, Haberle SG, Shen J, Xue B, Burrows M, et al (2017) Postglacial fire history and interactions with vegetation and climate in southwestern Yunnan Province of China. Clim Past 13: 613–627.

111. Ohneiser K, Ansmann A, Witthuhn J, Deneke H, Chudnovsky A, et al (2023) Self-lofting of wildfire smoke in the troposphere and stratosphere: simulations and space lidar observations. Atmos Chem Phy 23(4):2901-25.

112. Sun J, Tian B, Chen Z (2023) Effect of ozone addition and ozonolysis reaction on the detonation properties of $C_2H_4/O_2/Ar$ mixtures. Proc Combus 39(3):2797-806.

113. Ellis R, Palmer M (2016) Modulation of ice ages *via* precession and dust-albedo feedbacks. Geosci Frontiers 7(6):891-909.

114. Berger A, Yin Q (2012) Astronomical theory and orbital forcing. Sage Environ Change 1:405-25.

115. Viaggi P (2021) Quantitative impact of astronomical and sun-related cycles on the Pleistocene climate system from Antarctica records. Quaternary Sci Adv 4:100037.

116. Brown SK, Crosweller HS, Sparks RS, Cottrell E, Deligne NI, et al (2014) Characterisation of the Quaternary eruption record: analysis of the Large Magnitude Explosive Volcanic Eruptions (LaMEVE) databasis. J App Volcanol 3:1-22.

117. Gorkavyi N, Rault DF, Newman PA, Da Silva AM, Dudorov AE (2013) New stratospheric dust belt due to the Chelyabinsk bolide. Geophy Res Letters. 40(17):4728-33.

118. Brown P, Spalding RE, ReVelle DO, Tagliaferri E, Worden SP (2002) The flux of small near-Earth objects colliding with the Earth. Nature 420(6913):294-6.

119. Zhu D, Ciais P, Chang J, Krinner G, Peng S, et al (2018) The large mean body size of mammalian herbivores explains the productivity paradox during the Last Glacial Maximum. Nat Ecol Evol 2(4): 640–649.

120. Remsberg EE (2015) Methane as a diagnostic tracer of changes in the Brewer Dobson circulation of the stratosphere. Atmos Chem Phys 15: 3739–3754.

121. Andersen BG, Borns HW (2005) The ice age world: An introduction to quaternary history and research with emphasis on North America and Northern Europe during the last 2.5 million years. Scandinavian University Press.

122. Kaufman D, McKay N, Routson C (2020) Holocene global mean surface temperature, a multi-method reconstruction approach. Sci Data 7: 201.

123. Stephens DJ, Meuleners MJ, Van Loon H, Lamond MH, Telcik NP (2007) Differences in atmospheric circulation between the development of weak and strong warm events in the Southern Oscillation. J Climate 20(10):2191-209.

124. Paradiz B, Dilara P, Umlauf G, Bajsic I, Butala V. Dioxin emissions from coal combustion in domestic stove: formation in the chimney and coal chlorine content influence. Ther Sci 19(1):295-304.

125. Hossain SN, Bari S. Effect of different working fluids on shell and tube heat exchanger to recover heat from exhaust of an automotive diesel engine Linköping University Electronic Press.

126. Papapetrou M, Kosmadakis G, Cipollina A, La Commare U, Micale G (2018) Industrial waste heat: Estimation of the technically available resource in the EU per industrial sector, temperature level and country. App Ther Eng 138:207-16.

127. Cartapanis O, Bianchi D, Jaccard SL, Galbraith ED (2016) Global pulses of organic carbon burial in deep-sea sediments during glacial maxima. Nature communications 7(1):10796.

128. Davies JH, Davies DR (2010) Earth's surface heat flux. Solid earth 1(1):5-24.

129. Minton DA, Malhotra R (2007) Assessing the massive young Sun hypothesis to solve the warm young Earth puzzle. Astrophy J 660(2):1700.

130. Spalding C, Fischer WW, Laughlin G (2018) An orbital window into the ancient Sun's mass. Astrophy J Let 869(1):L19.

131. Wei W, Chen S, Wang Y, Cheng L, Wang X, et al (2022) The impacts of VOCs on PM2.5 increasing *via* their chemical losses estimates: A case study in a typical industrial city of China. Atmos Env 273: 118978.

132. Shaddick G, Thomas ML, Mudu P, Ruggeri G, Gumy S (2020) Half the world's population are exposed to increasing air pollution. NPJ Climate Atmos Sci3(1):1-5.

133. Bates NR, Johnson RJ (2023) Forty years of ocean acidification observations (1983–2023) in the Sargasso Sea at the Bermuda Atlantic Time-series Study site. Frontiers Marine Sci 10:1289931.

134. Dore JE, Lukas R, Sadler DW, Church MJ, Karl DM (2009) Physical and biogeochemical modulation of ocean acidification in the central North Pacific. Proceed Nat Acad Sci 106(30):12235-40.

135. Xie H, Wang F, Wang Y, Liu T, Wu Y, et al (2018) CO_2 mineralization of natural wollastonite into porous silica and CaCO 3 powders promoted *via* membrane electrolysis. Environ Earth Sci 77:1-0.

136. Calil PH, Richards KJ (2010) Transient upwelling hot spots in the oligotrophic North Pacific. J Geophys Res 115(C_2).

137. Polonskii A, Serebrennikov A (2020) Intensification of Atlantic and Pacific Large-Scale Upwelling under Recent Climate Conditions. Doklady Earth Sciences 492: 480-484.

138. Ohba T, Nakagawa M (2002) Minerals in volcanic ash 2: Non-magmatic minerals. Global Envi Res 6(2):53-60.

139. Kanji ZA, Ladino LA, Wex H, Boose Y, Burkert KM, et al (2017) Overview of ice nucleating particles. Meteorol Monographs. 58:1.

140. Pering TD, McGonigle AJ, Tamburello G, Aiuppa A, Bitetto M, et al (2017) A novel and inexpensive method for measuring volcanic plume water fluxes at high temporal resolution. Remote Sensing 9(2):146.

141. De Giacomo A, Dell'Aglio M, Salajkova Z, Vaníčková E, Mele D, et al (2022) Real-time analysis of the fine particles in volcanic plumes: A pilot study of laser induced breakdown spectroscopy with calibration-free approach (CF-LIBS). J Volcanol Geother Res 432:107675.

142. Durant AJ, Shaw RA, Rose WI, Mi Y, Ernst GG (2008) Ice nucleation and overseeding of ice in volcanic clouds. J Geophy Res Atmosph 113(D9).

143. Vestreng V, Myhre G, Fagerli H, Reis S, Tarrasón L (2007) Twenty-five years of continuous sulphur dioxide emission reduction in Europe. Atmosph Chem Phy 7(13):3663-81.

144. Western LM, Redington AL, Manning AJ, Trudinger CM, Hu L, et al (2022) A renewed rise in global HCFC-141b emissions between 2017-2021. Atmosph Chem Phy 22(14):9601-16.

145. Surl L, Roberts T, Bekki S (2021) Observation and modelling of ozone-destructive halogen chemistry in a passively degassing volcanic plume. Atmosph Chem Phy 21(16):12413-41.

146. Lu QB (2023) Critical review on radiative forcing and climate models for global climate change since 1970. Atmosphere 14(8):1232.

147. Bednarz EW, Hosseini, R, Chipperfield M (2023) Atmospheric impact of chlorinated very short-lived substances over the recent past -Part 2: Impacts of ozone. Atmosph Chem Phy 23: 13701-13711.

148. Holzworth RH, Brundell JB, McCarthy MP, Jacobson AR, Rodger CJ, et al (2021) Lightning in the Arctic. Geophy Res Lett 48(7):e2020GL091366.

149. Sun M, Liu D, Qie X, Mansell ER, Yair Y, et al (2021) Aerosol effects on electrification and lightning discharges in a multicell thunderstorm simulated by the WRF-ELEC model. Atmosph Chem Phy 21(18):14141-58.

150. Hardacre C, Palmer P, Engström K, Rounsevell M, Murray Rust D (2013) Probabilistic estimation of future emissions of isoprene and surface oxidant chemistry associated with land-use change in response to growing food needs. Atmosph Chem Phy 13.

151. Basu S, Mackey KR (2018) Phytoplankton as key mediators of the biological carbon pump: Their responses to a changing climate. Sustainability 10(3):869.

152. Trick CG, Bill BD, Cochlan WP, Wells ML, Trainer VL, et al (2010) Iron enrichment stimulates toxic diatom production in high-nitrate, low-chlorophyll areas. Proceed Nat Acad Sci 107(13):5887-92.

153. van Waveren I, Visscher H (1994) Analysis of the composition and selective preservation of organic matter in surficial deep-sea sediments from a high-productivity area (Banda Sea, Indonesia). Palaeogeo Palaeocli Palaeoecol 112(1-2):85-111.

154. Honjo S (1976) Coccoliths: Production, transportation and sedimentation. Marine Micropal 1:65-79.

155. Wells ML, Trainer VL, Smayda TJ, Karlson BS, Trick CG, et al (2015) Harmful algal blooms and climate change: Learning from the past and present to forecast the future. Harmful algae 49:68-93.

156. Radach G, Pätsch J (2007) Variability of continental riverine freshwater and nutrient inputs into the North Sea for the years 1977-2000 and its consequences for the assessment of eutrophication. Estuaries Coasts 30:66-81.

157. Copernicus ECMWF project.

158. Souza CM, Shimbo J, Rosa MR, Parente LL, Alencar A, et al (2020) Reconstructing three decades of land use and land cover changes in Brazilian biomes with landsat archive and earth engine. Remote Sensing 12(17): 2735.

159. Chiaka JC, Zhen L (2021) Land use, environmental, and food consumption patterns in Sub-Saharan Africa, 2000-2015: a review. Sustainability 13(15):8200.

160. Slot M, Winter K (2016) The effects of rising temperature on the ecophysiology of tropical forest trees. Adapt Res Changing Env 2016:385-412.

161. Makita N, Kosugi Y, Sakabe A, Kanazawa A, Ohkubo S, et al (2018) Seasonal and diurnal patterns of soil respiration in an evergreen coniferous forest: Evidence from six years of observation with automatic chambers. PLoS One 13(2):e0192622.

162. Langematz U (2019) Stratospheric ozone: down and up through the anthropocene. ChemTexts 5(2):8.

163. Lu QB (2022) Observation of large and all-season ozone losses over the tropics. AIP Advances 12(7).

164. Condamine FL, Silvestro D, Koppelhus EB, Antonelli A (2020) The rise of angiosperms pushed conifers to decline during global cooling. Proceed Nat Acad Sci117(46):28867-75.

165. Sternai P, Caricchi L, Pasquero C, Garzanti E, van Hinsbergen DJ, et al (2020) Magmatic forcing of Cenozoic climate?. J Geophy Res Solid Earth 25(1):e2018JB016460.